Journal of
Manufacturing and Materials Processing

MDPI

Review

A Review of Meltpool Dynamics and Grain Evolution in Inconel Alloys Produced by Laser Powder Bed Fusion

Sanjeevi Sharma R [1], Venkatachalaiah K N [1], Ramakrishna Pramod [2,*] and M. E. Shashi Kumar [3]

[1] Department of Physical Sciences, Amrita Vishwa Vidyapeetham, Bengaluru 560035, India; bl.ps.r4phy23001@bl.students.amrita.edu (S.S.R.); kn_venkatachalaiah@blr.amrita.edu (V.K.N.)
[2] Department of Robotics and Artificial Intelligence, Dayananda Sagar College of Engineering, Bengaluru 560111, India
[3] Department of Mechanical Engineering, Amrita Vishwa Vidyapeetham, Bengaluru 560035, India; me_shashikumar@blr.amrita.edu
* Correspondence: pramod-rai@dayanandasagar.edu

Abstract

Laser powder bed fusion (LPBF) is a disruptive additive manufacturing process for producing high-performance Inconel superalloy parts with complex shapes for the aerospace, energy, and other demanding industries. However, uniform part quality remains a persistent challenge, as process parameters, melt-pool dynamics, microstructural evolution, defect formation, and mechanical performance are closely coupled across a wide range of spatial and temporal scales. In previous reviews, these dimensions have been considered in isolation with limited insight into their interactions and implications for predictive process control. The present review aims to address this lacuna by proposing a unified Process–Structure–Property–Control (PSPC) framework for LPBF-produced Inconel 625, 718, and 738. The discussion begins with material attributes governing alloy processability, and then synthesises the melt-pool physics governing thermal behaviour, solidification, and energy transfer. Attention then turns to a critical assessment of grain evolution, defect formation, and process stability, showing how the thermal history governs microstructural development and, in turn, mechanical performance via linked process–structure–property relationships. Progress in multiscale numerical modelling, such as finite-element analysis, computational fluid dynamics, phase-field modelling, cellular automata, and phase-diagram calculation (CALPHAD), is reviewed to establish a comprehensive modelling ecosystem for predictive LPBF. The review also discusses the potential of emerging technologies, such as beam shaping, multi-laser processing, in situ monitoring, artificial intelligence, and powder recyclability, to increase the robustness and productivity of the process. Building on these advances, a digital-twin-enabled predictive-manufacturing framework that integrates physics-based models, data-driven algorithms, and real-time monitoring is introduced to enable closed-loop process optimisation. The review ends with a scientific synthesis and future research roadmap for intelligent, reliable, and autonomous LPBF of next-generation Inconel superalloys.

Keywords: additive manufacturing; digital twin; inconel alloys; laser powder bed fusion; melt-pool physics; multiscale modelling; process–structure–property–control framework

Check for updates

Academic Editor: Xiaoyu Liang

Received: 25 July 2026
Revised: 22 August 2026
Accepted: 30 August 2026
Published: 3 September 2026

Copyright: © 2026 by the authors. Licensee MDPI, Basel, Switzerland. This article is an open access article distributed under the terms and conditions of the Creative Commons Attribution (CC BY) license.

1. Introduction

Nickel-based superalloys have been among the most important materials for high-temperature structural applications for some time. Their strength, creep and fatigue

resistance, and endurance in the presence of oxidation and corrosion in harsh environments have made them a staple in the aerospace, energy, marine, and nuclear industries, where components must withstand intense heat and mechanical stress for long periods [1–4]. The Inconel family has attracted considerable interest because it can combine strength, thermal stability, and environmental durability. Furthermore, Inconel alloys are effective due to their chemistry and microstructural strengthening. These alloys are based on a nickel matrix (usually 50–70 wt.%) with additions of chromium, molybdenum, niobium, titanium, and aluminium, and are strengthened by solid-solution and precipitation hardening (γ' and γ'' phases). Every grade in the family has its own features. Inconel 625 offers excellent corrosion resistance and weldability, making it well suited to marine and chemical environments. Inconel 718 is the most widely used precipitation-hardenable grade, appreciated for its toughness and high-temperature strength. Inconel 738 was specifically designed for turbine blades and similarly demanding hot-section components, emphasising creep resistance and microstructural stability [5–9].

Inconel parts have been made for decades by casting, forging, machining, and welding. These routes have served industry well, but they do have real drawbacks. Coarse dendritic microstructures, elemental segregation, residual stress build-up, significant material waste, and limited design flexibility are drawbacks. These limitations are becoming harder to ignore as aerospace and energy applications require lighter, more geometrically complex components with shorter production lead times [10–12]. Additive manufacturing has thus evolved into a technology capable of solving many of these problems, with greater design freedom and better use of raw materials. Laser powder bed fusion (LPBF) is a widely used process for fabricating high-performance Inconel parts with complex geometries that traditional manufacturing methods cannot produce. Precise control of local thermal history enables process optimisation for tailoring microstructure and mechanical properties. However, the steep thermal gradients, complex melt-pool dynamics, and repeated thermal cycling inherent to LPBF, due to rapid melting and solidification, make process stability a critical challenge [13–17]. The interactions among process parameters, melt-pool behaviour, solidification conditions, and microstructural evolution determine the quality of Inconel components manufactured by LPBF. The crystallographic texture, defect formation, residual stress, and mechanical performance are controlled by the laser power, scan speed, hatch spacing, layer thickness, and scan strategy, which, in turn, determine melt-pool stability, cooling rate, and grain morphology. Hence, it is necessary to understand these interdependent process–structure–property relationships to obtain reproducible and defect-free components [18–21].

Recent advances in LPBF have significantly enhanced the understanding of the physical phenomena controlling the fabrication of Inconel alloy. Experimental studies aided by numerical simulations helped better define the relationships among processing conditions, thermal behaviour, microstructural evolution, and mechanical performance. Nevertheless, much of this work has been done in isolation, with individual studies examining specific aspects of the process, rather than how they all interact. Therefore, a complete picture of the process–structure–property relationship is still missing. Melt-pool dynamics have attracted the most attention among the different subjects studied due to their direct influence on the microstructure and defect evolution. Parameters such as laser power, scanning speed, hatch spacing, and layer thickness govern the energy input, melt-pool dimensions, thermal gradients, and cooling rates, which determine the quality of the final part [13,22]. The experimental work generally supports the view that increasing laser power enlarges the melt pool and enhances interlayer bonding, but the effect of increased energy input on defect generation is less clear. Across the reported studies, the consensus is that a stable melt pool is needed to produce high-density LPBF-fabricated Inconel components with

low residual stresses and minimal defect formation. Individual studies have tended to examine energy density, laser power, substrate preheating, powder characteristics, and scanning strategy in isolation, but they all point to the same fundamental mechanisms that operate through their effects on melt-pool geometry, thermal gradients, and solidification conditions. Optimised energy input leads to improved densification with reduced residual stresses, whereas excessive energy input causes melt-pool instability, keyhole formation, and increased porosity. Likewise, substrate preheating improves melt-pool stability by decreasing thermal gradients and suppressing thermal fluctuations. That said, it is difficult to determine the relative contribution of any one process parameter. This is because the studies under review use different machine platforms, powder feedstocks and processing windows, limiting the degree to which direct comparison is possible. Collectively, these findings suggest that melt-pool stability is driven by the interaction of processing parameters rather than any single parameter, highlighting the need for holistic optimisation approaches that deliver consistent part quality [1,13,22].

Melt-pool behaviour directly influences solidification mechanisms and the development of grain structure. The transition from columnar to equiaxed grain growth has been studied extensively. It is found to depend on the competition between the thermal gradient and the solidification rate, with implications for crystallographic texture, anisotropy, and mechanical performance [18–21]. While rapid cooling generally leads to finer grains and higher strength, it has been shown that similar processing conditions can result in significantly different grain morphologies depending on alloy composition, scan strategy and cyclic thermal history. This variability shows that grain evolution cannot be explained by cooling rate or energy density alone, but is a manifestation of the coupled interplay between melt-pool dynamics, heat transfer, and solidification behaviour. Therefore, predicting microstructural evolution requires a combined thermal and metallurgical analysis rather than isolated experimental observations. Defect formation remains one of the biggest hurdles to the broader industrial use of LPBF for critical Inconel components. Distinct physical mechanisms cause lack-of-fusion defects, keyhole porosity, balling, and microcracks, and their evolution with processing parameters differs. Low energy input can cause incomplete melting and lack-of-fusion defects, while high energy density can result in unstable keyhole behaviour and gas porosity. These seemingly contradictory results suggest that defect generation is, at heart, a question of process stability rather than a single processing variable. Therefore, several recent studies have focused on identifying robust processing windows that minimise defects while maintaining favourable thermal conditions and microstructural refinement [13,22,23].

In addition to microstructure and defects, thermomechanical effects play a significant role in the structural integrity of LPBF-built parts. The layer-by-layer fabrication results in rapid, repeated heating and cooling cycles, leading to large thermal gradients. These thermal gradients cause non-uniform expansion and contraction, leading to residual stresses, distortion, and possible crack initiation [13,24,25]. Techniques such as optimised scan patterns, substrate preheating, stress-relief heat treatments, and hot isostatic pressing have all demonstrated measurable benefits. However, their efficacy varies greatly with component geometry, alloy composition, and processing conditions. This indicates that the evolution of residual stresses is not only a post-processing issue but also an intrinsic result of the coupled thermal and metallurgical processes that occur during LPBF. Much effort has been devoted to computational modelling of LPBF to improve predictive ability. Finite-element methods, computational-fluid dynamics, phase-field modelling, and multiscale simulation techniques have all made important contributions to understanding heat transfer, melt-pool behaviour, solidification, and stress development [26,27]. However, these approaches have largely been developed in parallel and operate at different

spatial and temporal scales. Thermal models often ignore grain evolution; microstructure models often simplify melt-pool fluid flow or mechanical response; and thermomechanical simulations often employ simplified thermal histories that do not capture transient melt-pool behaviour. Recent multiscale modelling frameworks have made significant progress toward integrating these phenomena. However, truly comprehensive coupling across processing parameters, thermo-fluid behaviour, microstructural evolution, defect formation, and mechanical performance remains limited.

Considerable advances have been made in understanding melt-pool thermofluid behaviour, solidification mechanisms, grain evolution, defect formation, residual-stress development, mechanical performance, and computational modelling in LPBF of Inconel alloys, but these issues have largely been studied separately. As a consequence, the direct correlation between processing parameters, melt-pool dynamics, microstructural evolution, defect formation and residual stress, thermomechanical response, and component performance is only partially understood, which limits the predictive capability of current optimisation strategies. These gaps underline the need for a unified framework that combines experimental observations, multiscale modelling and process–structure–property relationships into a coherent methodology for predictive LPBF of Inconel alloys.

Computational modelling has made some progress in closing these gaps by predicting thermal history, stress evolution, and microstructural behaviour. However, most modelling approaches are still limited to specific physical phenomena or spatial and temporal scales. Grain evolution is often neglected in thermal models, realistic melt-pool fluid flow is rarely considered in phase-field simulations, and simplified thermal histories are typically used in thermomechanical analyses, which cannot fully capture the transient nature of LPBF processing [26,27]. In addition, although the influence of processing parameters on microstructure and defects has been reported in numerous experimental studies, there are no standard datasets for validating predictive models. The absence of fully integrated modelling and experimental frameworks hinders the development of reliable process optimisation strategies for different Inconel alloy systems.

As shown in Table 1, previous reviews mainly considered melt-pool physics, process–property relationships, or computational modelling as separate research topics. To the best of the authors' knowledge, there is no comprehensive review that provides a closed-loop view of process parameters → melt-pool dynamics → grain structure evolution → defect formation → residual stress and distortion → mechanical behaviour → digital twin-assisted monitoring and feedback control in a systematic manner. This has limited understanding of the process, hindering the establishment of predictive relationships to enable efficient process optimisation and adaptive manufacturing of LPBF-fabricated Inconel components.

Table 1. Scope of this review with a comparison of representative review articles on LPBF of Inconel alloys.

Review	Scope	Key Contributions	Remaining Limitations
Karia et al. (2017) [2]	Selective Laser Melting (SLM) of Inconel alloys	Introduced SLM fundamentals, process parameters, and early applications of Inconel alloys	Published before recent developments in multiscale modelling, in situ monitoring, digital twins, and AI-assisted manufacturing
Volpato et al. (2022) [1]	LPBF of Inconel superalloys	Comprehensive review of process parameters, microstructure, defects, and mechanical properties	Limited integration of thermo-fluid behaviour, multiscale modelling, intelligent monitoring, and closed-loop process optimisation

Table 1. *Cont.*

Review	Scope	Key Contributions	Remaining Limitations
Sarkar et al. (2024) [27]	Computational modelling of LPBF	Comprehensive review of finite-element modelling techniques and computational strategies for LPBF	Focuses mainly on modelling methodologies, with limited discussion of experimental validation, grain evolution, defect mechanisms, and digital manufacturing
Present Review	Integrated PSPC framework	Systematically connects process parameters, melt-pool dynamics, grain evolution, defect formation, residual stress, mechanical behaviour, multiscale modelling, digital twins, and AI-assisted process control within a unified framework	Provides a comprehensive roadmap for predictive, physics-informed, and closed-loop optimisation of LPBF-fabricated Inconel alloys

To address these gaps, this review presents a unified PSPC framework for LPBF of Inconel alloys (Figure 1) that integrates processing parameters, melt-pool dynamics, grain evolution, defect formation, residual-stress development, mechanical behaviour, and digital-twin-assisted feedback control into a single predictive structure. The proposed PSPC framework bridges these previously disjointed research areas. It offers a consistent process–structure–property relationship for the scientific foundation of predictive process optimisation and intelligent manufacturing of LPBF-fabricated Inconel components.

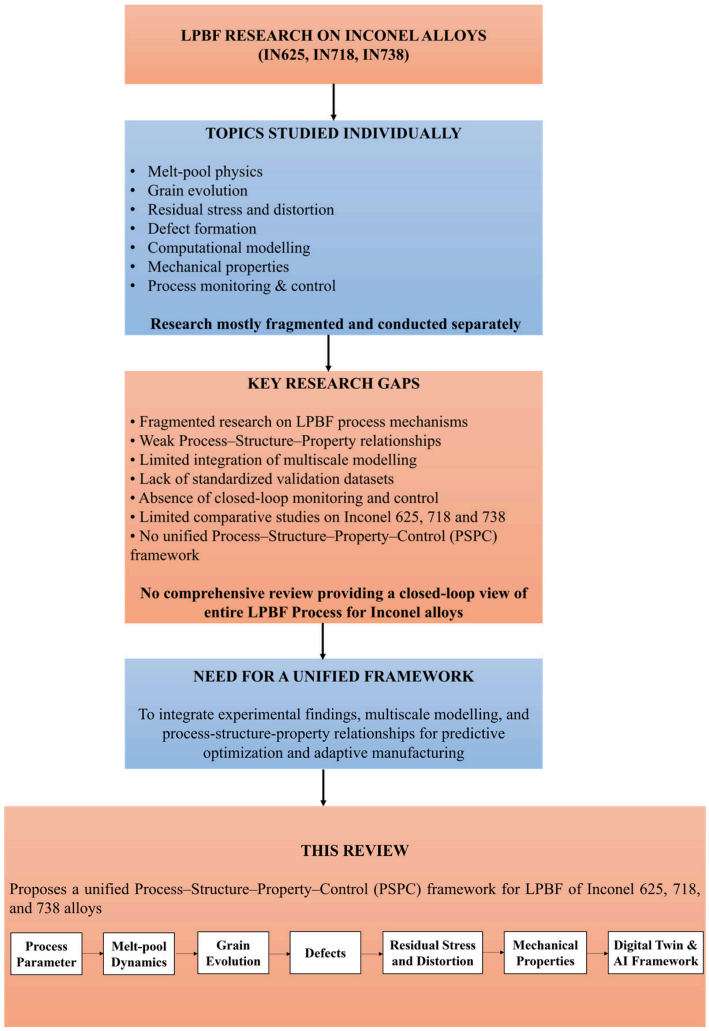


Figure 1. Research gaps in LPBF processing of Inconel alloys identified from the existing literature (synthesised from Refs. [1,2,13,14,16–27]).

This review systematically consolidates the current understanding of LPBF processing of Inconel 625, 718, and 738 alloys, building on the unified PSPC framework shown in Figure 1. In contrast to earlier reviews, which treat individual topics in isolation, the current work couples melt-pool thermofluid behaviour, solidification mechanisms, grain evolution, defect formation, residual-stress evolution, and mechanical performance into a unified PSPC relationship. In addition, recent advances in in situ monitoring, digital twin technologies, and physics-informed artificial intelligence are critically evaluated alongside finite element, computational fluid dynamics, phase-field, CALPHAD, and multiscale modelling approaches. This review synthesises previously isolated areas of research to establish a comprehensive scientific basis for the predictive, physics-based, and closed-loop optimisation of LPBF-fabricated Inconel alloys.

2. Materials and Methods

2.1. Material Systems for LPBF Processing

Nickel-based superalloys are among the most relevant material families for laser powder bed fusion (LPBF) due to their superior combination of high-temperature strength, corrosion and oxidation resistance, and long-term microstructural stability. Inconel 625, Inconel 718, and Inconel 738 have been extensively studied due to their widespread use in aerospace, power generation, and gas-turbine applications where components are often exposed to severe thermo-mechanical loading. However, all three belong to the same alloy family. Yet, they vary in composition, strengthening mechanisms, and thermophysical behaviour, leading to substantially different melt-pool dynamics, solidification responses, defect behaviour, and mechanical outcomes during LPBF [28–31]. The success of producing LPBF parts depends on both the process parameters and the material's intrinsic properties. Laser irradiation leads to rapid melting and re-solidification under steep thermal gradients with cooling rates typically in the range of 10^5–10^6 Ks^{-1}. Complex interactions among heat transfer, fluid dynamics, phase transformation, and solidification occur under these extreme conditions, all of which are strongly influenced by alloy chemistry. The composition directly affects the stability of the melt pool, grain development, element partitioning, tendency to crack, and response to precipitation, all of which ultimately determine the quality of the component and its performance in service [30–33].

Among the three alloys, Inconel 625 shows the best LPBF processability. Solid-solution strengthening, mainly due to additions of molybdenum and niobium, provides good corrosion resistance and a relatively wide processing window. However, excessive laser energy input can destabilise the melt pool, resulting in spatter, keyhole porosity, and elemental segregation, all of which can degrade fatigue performance and dimensional precision [34–37]. Inconel 718 is the most studied LPBF alloy in the literature. With suitable heat treatment, precipitation hardening by the γ'' and γ' phases provides an excellent combination of strength, ductility, and high-temperature performance. The LPBF processing of this alloy typically exhibits stable melt-pool behaviour and a relatively wide processing window. However, the microstructural results are sensitive to the thermal history, residual-stress build-up and post-processing conditions. Heat treatment is especially important for dissolving non-equilibrium phases and activating precipitation strengthening, thereby greatly enhancing mechanical properties and fatigue resistance [29,38–43]. Inconel 738 is the most difficult of the three to work with. The high fraction of the γ' precipitate provides excellent creep performance but limits weldability and increases the susceptibility to hot cracking under the thermal stresses imposed during rapid solidification. Consequently, producing Inconel 738 without defects needs tighter processing windows, more accurate laser parameter optimisation, and better thermal management strategies [28,44–46]. However, some processing behaviour is common to all three alloys. Melt-pool stability systematically

controls grain morphology, defect formation, residual-stress evolution, and mechanical performance. Conduction-mode melting usually produces dense parts with fine-grained, cellular, or columnar microstructures when the proper amount of energy input is used; however, too little results in lack-of-fusion defects, and too much results in keyhole porosity. Therefore, true LPBF optimisation requires the concurrent consideration of both alloy chemistry and process parameters, neither of which can be considered independently. A direct comparison of the LPBF behaviour of the three alloys, including representative processing windows, melt-pool regimes, microstructural evolution, dominant defect mechanisms, and associated mechanical implications, is presented in Table 2 [28–51].

Table 2. Representative LPBF processing windows, melt-pool regimes, microstructural characteristics, dominant defect mechanisms, and corresponding mechanical performance outcomes for Inconel 625, Inconel 718, and Inconel 738 alloys [28–51].

Material	Typical LPBF Processing Window	Dominant Melt-Pool Regime	Predominant Microstructure	Major Defect Mechanisms	Dominant Strengthening Mechanism	Mechanical Implications
Inconel 625	180–250 W, 700–1100 mm/s, VED 50–80 J/mm^3	Stable conduction	Fine cellular-dendritic columnar γ matrix	Negligible porosity under well-controlled conditions; elevated VED encourages spatter and keyhole pore formation	Solid-solution strengthening via Mo and Nb additions	Good tensile strength combined with high ductility and corrosion resistance
Inconel 625	Below 180 W, above 1100 mm/s, VED below 40 J/mm^3	Lack-of-fusion	Fragmented melt tracks with poorly defined grain boundaries	Lack of fusion voids and weak interlayer adhesion	Incomplete part densification	Degraded tensile strength and reduced fatigue resistance
Inconel 625	Above 250 W, below 600 mm/s, VED above 90 J/mm^3	Keyhole	Coarsened dendritic morphology	Keyhole pores and localised elemental segregation	Localised overheating effects	Diminished fatigue life and loss of dimensional precision
Inconel 718	200–350 W, 600–1000 mm/s, VED 60–100 J/mm^3	Stable conduction	Fine columnar γ dendrites developing γ″ precipitation upon post-build ageing	Minor gas-induced porosity	Precipitation strengthening through γ″ and γ′ phases	Elevated strength and reliable fatigue behaviour following heat treatment
Inconel 718	Below 180 W, above 1000 mm/s, VED below 50 J/mm^3	Lack-of-fusion	Non-uniform grain morphology	Large unfused pores and incomplete interlayer bonding	Insufficient energy for full melting	Reduced part density and lower tensile strength
Inconel 718	Above 350 W, below 500 mm/s, VED above 110 J/mm^3	Keyhole	Coarsened columnar grain structure	Keyhole porosity accompanied by Nb-rich segregation zones	Excessive thermal input	Shortened fatigue life and diminished dimensional accuracy
Inconel 738	200–300 W, 500–900 mm/s, VED 60–90 J/mm^3	Stable conduction	Columnar dendrites with distributed γ′ precipitates	Low-level residual porosity	γ′ precipitation strengthening	Outstanding creep resistance and retained strength at elevated temperatures
Inconel 738	Below 180 W, above 900 mm/s, VED below 50 J/mm^3	Lack-of-fusion	Irregular and poorly developed dendritic structure	Lack-of-fusion defects and incomplete metallurgical bonding	Insufficient inter-track consolidation	Reduced mechanical strength across loading conditions

Table 2. *Cont.*

Material	Typical LPBF Processing Window	Dominant Melt-Pool Regime	Predominant Microstructure	Major Defect Mechanisms	Dominant Strengthening Mechanism	Mechanical Implications
Inconel 738	Above 320 W, below 500 mm/s, VED above 100 J/mm^3	Keyhole	Coarsened dendritic structure	Hot cracking combined with keyhole porosity	High susceptibility to thermally induced cracking	Degraded creep life and compromised structural integrity

2.2. Influence of Powder Characteristics on Melt-Pool Dynamics and Grain Evolution

Powder characteristics affect LPBF beyond feedability alone, since they dictate powder-bed uniformity and the conditions governing laser-energy transfer to the material. Particle-size distribution controls the balance between packing and melting response; excessive fines can compromise flowability and encourage agglomeration, while coarse particles demand greater energy for complete fusion. Likewise, predominantly spherical particles tend to favour uniform spreading, whereas irregular particles and satellites raise inter-particle friction and introduce local packing variation. Particle size, morphology, and flowability must therefore be treated jointly rather than in isolation, as their combined effect sets powder-bed consistency and contributes to melt-pool stability [1,30].

These variations in powder-bed condition carry through into solidification and grain development via changes in local melt-pool thermal history. Non-uniform spreading or fluctuations in powder-layer thickness can alter melting conditions, modifying the thermal gradients and cooling behaviour that govern epitaxial growth, grain morphology, and crystallographic texture [39,47]. Repeated powder reuse can further alter surface condition, particle morphology, and flow behaviour, adding further variability to melt-pool stability and the resulting solidification response [30]. Powder characteristics thus function as an upstream variable within the process–structure relationship, exerting their influence on grain evolution primarily through melt-pool behaviour rather than through powder properties in isolation. This also explains why no universally optimal powder condition can be defined independently of alloy composition, layer thickness, and laser-processing parameters [1,30,39,47].

Comparative data are provided in Table 2, which show that the combined effects of process parameters, alloy composition, and melt-pool stability determine LPBF processability. Across the reviewed studies, stable processing is generally achieved within volumetric energy density (VED) ranges of approximately 50–80 J/mm^3 for Inconel 625, 60–100 J/mm^3 for Inconel 718, and 60–90 J/mm^3 for Inconel 738. In contrast, VED values below approximately 40–50 J/mm^3 frequently result in lack-of-fusion defects due to insufficient melting, whereas values exceeding approximately 90–110 J/mm^3 promote keyhole instability, excessive vaporisation, elemental segregation, and pore formation. However, the differences between the Inconel 625, 718, and 738 processing windows are related to differences in strengthening mechanisms and thermophysical properties, but all three alloys follow the same basic melt-pool transitions: from lack of fusion to stable conduction to keyhole melting with increasing energy input [30,32,36,37,43,51]. These quantitative processing windows provide practical guidelines for parameter selection but should not be interpreted as universal optimisation criteria, since machine architecture, laser spot size, layer thickness, hatch spacing, and powder characteristics significantly influence the effective energy delivered to the melt pool. These results establish the melt-pool behaviour as the main bridge between process parameters and the resulting microstructure, defect population, and mechanical response. Thus, a good understanding of melt-pool thermo-fluid dynamics is essential to develop reliable process–structure–property relationships in LPBF of Inconel alloys. The

following section presents an integrated melt-pool physics framework that includes heat transfer, fluid flow, keyhole physics, and solidification mechanisms, collectively controlling LPBF processing.

3. Unified Melt-Pool Physics Framework

The evolution of the melt pool in LPBF of Inconel alloys is the fundamental physical link between processing parameters, thermal behaviour, solidification conditions, microstructural development, defect formation, and mechanical performance. The thermal energy incident on the powder bed depends on laser power, scan speed, hatch spacing, and layer thickness. The melt-pool response is a function of the efficiency with which that energy is absorbed and transferred within the material. Laser absorptivity, beam profile, powder properties, thermal accumulation, recoil pressure and melt-pool fluid flow affect process stability. Therefore, VED in LPBF of Inconel alloys should be viewed as a first-order descriptor, and not an exhaustive predictor of melt-pool stability, microstructure, or defect formation [52–55]. The governing physics can then be viewed as a sequential cascade in which primary processing parameters first determine the absorbed energy, which in turn controls the melt-pool flow, local solidification conditions and ultimately the resulting microstructure and defect population, as shown in Figure 2.

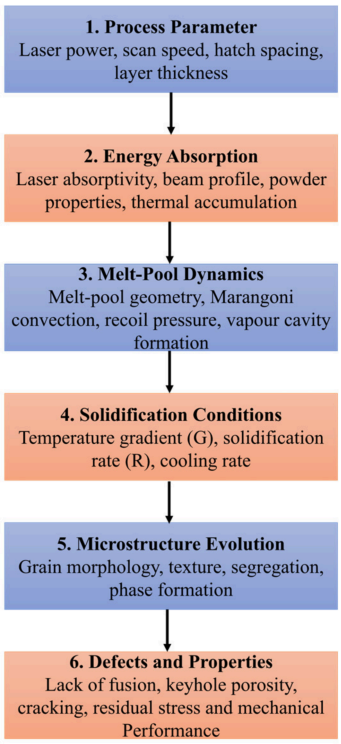


Figure 2. A unified melt-pool physics framework outlining the hierarchical connections between LPBF processing parameters, energy absorption, melt-pool dynamics, solidification conditions, microstructural evolution, and defect formation in Inconel alloys [52–57].

Three characteristic melt-pool regimes are consistently observed in LPBF processing of Inconel 625, Inconel 718, and IN738LC. Insufficient energy input results in incomplete melting, manifested as discontinuous melt tracks and poor layer bonding. As absorbed energy increases, a stable conduction regime is established, with continuous melt pools, uniform heat distribution, controlled solidification, and near-full-density builds. Further increases in surface temperature promote vaporisation and the development of a vapour depression. During conduction-dominated melting, energy absorption is primarily governed

by a single Fresnel interaction at the melt surface, with the absorbed fraction depending on the angle of incidence and the alloy's temperature-dependent optical properties, typically yielding an absorptivity well below unity. As the surface temperature approaches the vaporisation point and a depression begins to form, this single-bounce geometry breaks down. Laser rays that would otherwise be reflected away from a flat surface instead strike the curved cavity wall at a steeper local angle, are partially absorbed, and are redirected onto a neighbouring section of wall further down the depression, where a further fraction is absorbed. This cascading, multiple-reflection process raises the effective absorptivity substantially above the conduction-mode value, concentrating additional energy preferentially near the base and lower walls of the depression, where repeated trapping is most probable [51,52,56]. The resulting local heating reinforces vaporisation at these sites, deepening the depression further and progressively transitioning melting into the keyhole regime.

Keyhole stability is subsequently governed by the dynamic balance between evaporation-induced recoil pressure, which sustains the vapour depression, and restoring forces, mainly surface tension and capillary pressure, as well as hydrostatic and melt-flow effects [51,52,56,57]. Consistent with observations of keyhole formation in laser powder bed fusion, the recoil pressure increases exponentially with increasing surface temperature. It is reinforced by multiple internal reflections that concentrate energy on the rear keyhole wall [58]. Following the classical thermodynamic treatment of evaporation-driven recoil pressure, this behaviour can be expressed as a fraction of the local saturated vapour pressure at the keyhole wall:

$$P\_r(T) = A \cdot P\_sat(T) \quad (1)$$

where A is a numerical coefficient that, for practical values of ambient pressure, is close to its minimal value of 0.55 [59]. The saturated vapour pressure P_sat(T) itself follows a kinetic-theory-based exponential dependence on surface temperature:

$$P\_sat(T) = B_0 T^{-1/2} \exp\left(\frac{-U}{T}\right) \quad (2)$$

where B_0 is a vaporisation constant specific to the evaporating species, and U = (M_a·L_v)/(N_a·k_b), with M_a the atomic mass, L_v the latent heat of evaporation, N_a Avogadro's number, and k_b Boltzmann's constant [59]. Because B_0 and L_v differ substantially between the constituent elements of Inconel 625, Inconel 718, and IN738LC, most notably in chromium relative to nickel and iron, this pair of relations directly shows why identical local surface temperatures do not translate into identical recoil pressures across the three alloys. The absorbed energy delivered through the multiple-reflection mechanism described above raises T at the keyhole wall, and P_r(T) rises correspondingly, so the recoil-pressure term feeding the force balance is inherently composition-dependent rather than a fixed function of VED alone.

Disturbance of the balance between P_r(T) and the restoring surface-tension, capillary and hydrostatic terms can induce keyhole oscillation and collapse, resulting in vapour or gas entrapment and keyhole porosity. Although the underlying mechanism is common to Inconel 625, Inconel 718, and IN738LC, its magnitude is alloy-dependent because differences in composition and constituent-element volatility influence vapourisation behaviour. Elements with comparatively high vapour pressure at a given temperature, such as chromium relative to nickel or iron, evaporate preferentially from the melt surface, so the vapour leaving the depression is not compositionally representative of the bulk alloy. This preferential evaporation modifies the local vapour-plume composition and, in turn, the effective P_sat(T) governing recoil pressure in the force balance, shifting the VED threshold at which oscillation and collapse occur for a given alloy. Accordingly, comparable VED

values do not necessarily produce identical melt-pool responses across these alloys, and the resulting keyhole porosity susceptibility of Inconel 625, Inconel 718, and IN738LC must be interpreted in light of alloy-specific vapour-pressure behaviour rather than VED magnitude alone [50,54,55,60,61].

Melt-pool dynamics determine the local temperature conditions that govern solidification behaviour. The temperature gradient (G) and solidification rate (R) collectively determine the stability of the advancing solidification front and influence grain morphology during rapid solidification. The thermal variables stem directly from melt-pool evolution; hence, alterations in processing parameters affect the final microstructure indirectly via changes in melt-pool shape, fluid dynamics, and heat transfer rather than solely through volumetric energy density. Both numerical models and experimental investigations consistently reveal that local temperature gradients, cooling rates, and melt-pool shape together influence grain evolution and defect susceptibility in nickel-based superalloys [53,57,62–66].

This unified melt-pool framework provides the conceptual basis for the rest of this review. Thus, the following sections interpret processing windows, microstructural evolution, and defect formation in terms of the melt-pool regimes established here, without revisiting the individual mechanisms of lack-of-fusion, stable conduction or keyhole melting at each stage. The three fundamental melt-pool regimes are common to LPBF processing of Inconel 625, Inconel 718, and IN738LC. However, the joint effects of alloy chemistry, thermal properties, energy absorption, melt-pool dynamics, and solidification behaviour govern the transitions between them. For these alloys, the position and size of each regime differ, as differences in composition and solidification response influence melt-pool stability, defect susceptibility, and the resulting microstructure. However, the fundamental physics of the melt pool is similar across all Inconel alloys. It provides a common framework for discussing the alloy-specific processing–microstructure–property relationships, which are discussed in the following sections [55,60,65,67–71]. Table 3 summarises the characteristic processing conditions, dominant physical mechanisms, and typical outcomes of each regime, providing a reference framework for a comparative discussion of the LPBF processing behaviour of Inconel 625, Inconel 718, and IN738LC in the remainder of this review.

Table 3. Unified melt-pool regime framework for LPBF of Inconel alloys [52,54–56,60,61].

Melt-Pool Regime	Typical Processing Condition (Qualitative)	Dominant Physical Mechanism	Typical Outcome
Low Energy (Under-melting)	Inadequate absorbed energy	Incomplete melting and discontinuous melt-track formation	Lack-of-fusion defects, poor interlayer bonding, reduced part density
Stable Conduction	Balanced absorbed energy	Continuous melt pool sustained by controlled heat transfer and fluid flow	Near-full density, homogeneous microstructure, enhanced mechanical properties
Keyhole	Excessive absorbed energy	Vapour cavity generation, recoil pressure development, and unstable melt-pool flow	Keyhole porosity, gas entrapment, diminished process stability

The melt-pool regimes reported in Table 3 provide a consistent foundation for discussing the LPBF processing behaviour of Inconel 625, Inconel 718, and IN738LC. The precise boundaries of the processing window are alloy-specific and depend on thermal properties and solidification behaviour, but the fundamental transition from undermelting to stable conduction to keyhole melting is common to the three alloys. This integrated framework provides the physical basis for explaining, in the following sec-

tions, the influence of processing parameters on grain evolution, defect formation, and mechanical properties.

4. Grain Evolution Mechanisms

4.1. Epitaxial Column Growth

The primary grain morphology development during solidification is controlled by extreme conditions of 10^4–10^7 K/m thermal gradients and cooling rates of similar magnitude in laser powder bed fusion. Under these conditions, epitaxial solidification dominates grain growth, with partially melted grains from the underlying layer acting as templates that control the crystallographic orientation of the newly solidified material. The solidification front preferentially progresses along the existing orientation in the substrate below, leading to elongated columnar grains that extend over several deposited layers rather than nucleating new grains with random orientations. This epitaxial mechanism controls the initial microstructural architecture, which affects texture development, defect formation, and mechanical anisotropy in LPBF-built nickel-based superalloys [72–76]. The formation of epitaxial columnar grains depends on the interaction between the temperature gradient G and the solidification rate R. At high G/R ratios, the solidification front is stable, and the dendrites grow directionally, parallel to the dominant heat-extraction path, which usually coincides with the build direction. The underlying grains largely retain their crystallographic orientation because each thermal cycle remelts only the uppermost layer. This initiates a competitive grain-growth process, in which dendrites with favourable orientations continue to grow, while those with less favourable orientations are gradually suppressed. The outcome is a microstructure of long columnar grains with a pronounced ⟨001⟩ texture, a characteristic feature often observed for LPBF-processed nickel superalloys [72,74,77–79].

Epitaxial growth occurs in all LPBF-processed Inconel alloys, but the extent of it depends on alloy composition, solidification characteristics and heat-transport behaviour. For example, Inconel 625 tends to exhibit relatively stable epitaxial growth, with a wider processing window and lower sensitivity to solidification cracking. Steady directional heat removal favours elongated cellular-columnar dendrites along the build direction, and rapid cooling rates leave fine cellular substructures within these columnar grains. However, changes in the scan strategy or the local thermal environment can disrupt this epitaxial continuity, resulting in finer grains and weaker texture [73,80–82]. In contrast, Inconel 718 has a hardened microstructure due to precipitation and is more sensitive to thermal history, which clearly shows greater competitive grain selection. In typical LPBF processing, steep thermal gradients promote sustained columnar growth across multiple layers, resulting in a microstructure with a strong directional texture along the build axis. However, variations in hatch spacing, scan rotation, or melt-pool shape can easily disturb epitaxial stability. Localised disturbances to heat flow in specific regions disrupt directional solidification, reduce the grain aspect ratio, and lead to more heterogeneous grain structures, offering a practical method to tune microstructural anisotropy without altering the alloy composition [74,76,83–86].

Among the three alloys, Inconel 738 has the highest directional solidification tendency owing to its high γ' content, narrow processing window, and poor weldability. The high thermal gradients in LPBF lead to rapid epitaxial growth of columnar dendrites along the build direction, which causes marked crystallographic texture but also enhances the susceptibility to strain localisation and solidification cracking. Therefore, control of epitaxial growth is of particular importance in Inconel 738, since uninterrupted columnar continuity can promote crack initiation during solidification. Recent studies have demonstrated that proper control of melt-pool thermal behaviour and scan strategy can partially break up

epitaxial growth, refine grain structure, and improve structural integrity while maintaining high-temperature performance [75,87–91]. The characteristic laser-scan tracks and the overlapping melt-pool morphology during LPBF processing are shown in Figure 3a–d. Partial remelting of adjacent passes and successive layers provides metallurgical continuity between passes while maintaining the steep thermal gradients that control the directionality of heat flow. These thermal conditions underpin the epitaxial grain growth mechanism, which is also directly reflected in the long columnar grains shown in Figure 3e,f [92]. Epitaxial columnar growth usually dictates solidification in LPBF; however, variations in heat gradient, melt-pool dynamics, and scanning method can disrupt this directed process, promoting equiaxed grain formation instead. The columnar-to-equiaxed transition (CET) is pivotal for grain refinement, texture development, and the extent of microstructural isotropy, and constitutes the primary subject of the ensuing discussion [72,75,77].

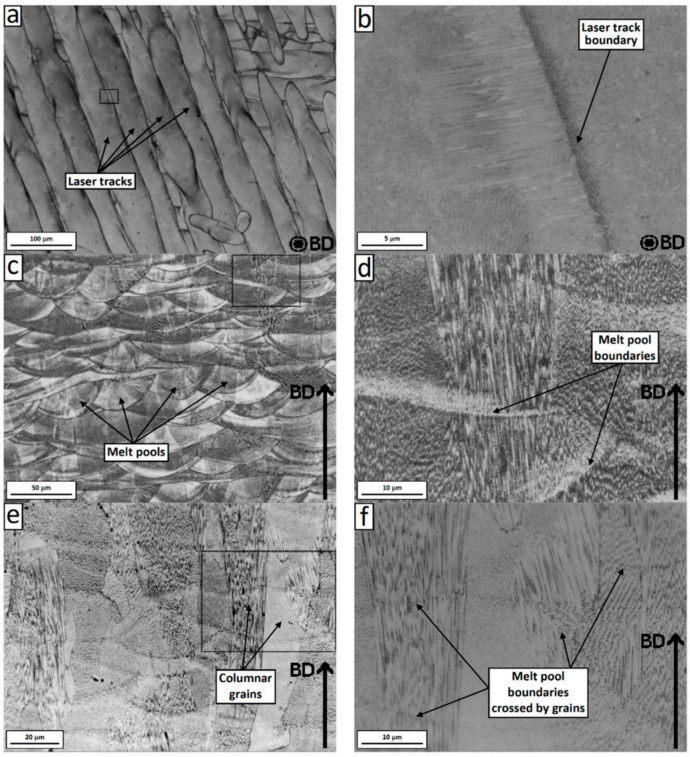


Figure 3. Optical microscope (OM) images of the electrochemically etched SLM Inconel 718 sample showing the track-to-track melt-pool boundaries (MPBs) on the horizontal plane at standard and high magnification (**a**,**b**), and arc-shaped MPBs on the vertical plane at both magnification levels (**c**,**d**). Columnar grains extending through several layers at standard and high magnification, respectively, in further OM images of the same alloy etched by Kalling's reagent on the vertical plane (**e**,**f**) [92].

4.2. Columnar to Equiaxed Transition (CET)

The CET is a critical microstructural feature in LPBF that controls the nature of grain growth, either directional growth or a switch to heterogeneous nucleation during solidification. Epitaxial columnar growth dominates when thermal gradients are steep. CET occurs when the solidification front becomes unstable, allowing new grains to nucleate ahead of the advancing interface. The transition depends primarily on the interaction between the temperature gradient G and the solidification rate R, as well as on constitutional supercooling, convective flow in the melt pool, alloy chemistry, and local thermal history. Therefore, CET is a viable approach to alter grain morphology, decrease crystallographic texture, and enhance isotropy for LPBF-fabricated Inconel alloys [72,77,93]. A schematic of

the CET mechanism is shown in Figure 4a. The key processing variables controlling the CET are summarised in Figure 4b.

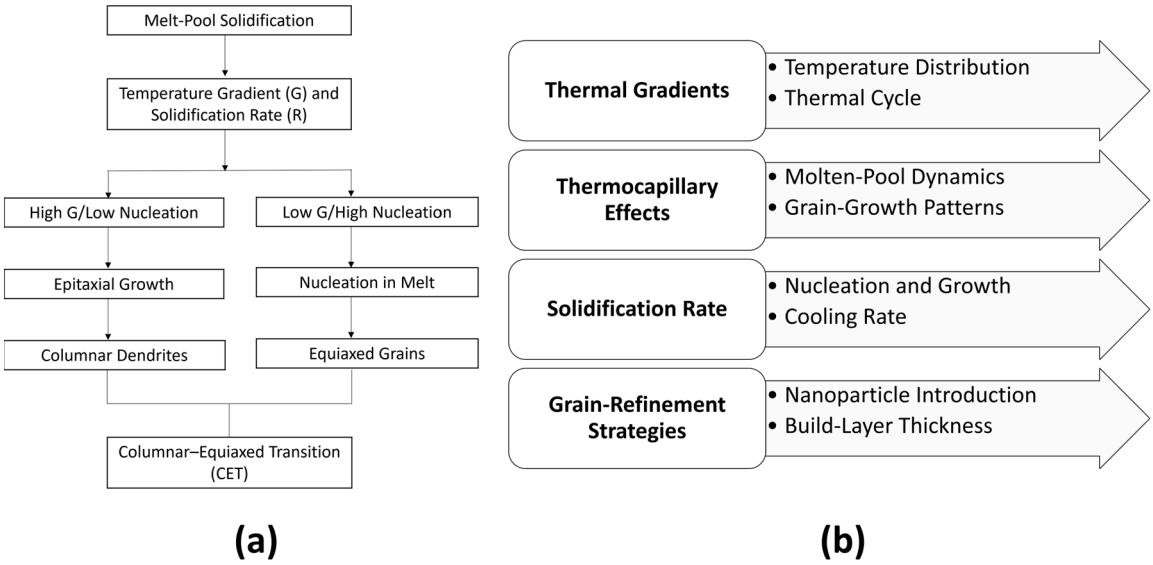


Figure 4. (**a**) Mechanism of CET transition, (**b**) factors influencing columnar to equiaxed transition in LPBF.

The conventional G/R criterion provides only a first-order description of CET because LPBF cooling rates of approximately 10^5–10^7 K s^{-1} impose strong non-equilibrium solidification conditions [57,64,65]. Restricted solute diffusion causes enrichment of the liquid ahead of the advancing interface, locally depresses the liquidus temperature, and increases constitutional supercooling. CET therefore requires not simply a reduction in G/R, but sufficient nucleation undercooling and viable heterogeneous nuclei capable of competing with epitaxial growth [57,72,94,95]. The distinct contributions of G and R should be separated: a high temperature gradient stabilises directional heat extraction and favours columnar growth, whereas an increasing solidification rate drives greater departure from local equilibrium and promotes undercooling ahead of the interface. On this basis, the G/R ratio serves as a first-order indicator of interface morphology, while the G × R product represents the local cooling rate and governs mainly cellular/dendritic refinement. However, neither quantity alone is sufficient to define CET, since the transition also depends on nucleation undercooling (ΔT_n), the density of heterogeneous nucleation sites (N_0), and composition-dependent solutal growth restriction [96,97].

This interdependence rules out a single universal critical G/R value applicable to IN625, IN718, and IN738/IN738LC. Variations in Nb, Mo, Al, and Ti partitioning shift constitutional undercooling, effective freezing behaviour, and the position of the CET boundary within the G–R space. Sensitivity analysis of Ni-based superalloys has additionally shown that nucleation density can influence CET more strongly than individual compositional parameters, indicating that thermal and solutal contributions cannot be assigned a fixed, uniform weighting [97]. Quantitative data indicate that LPBF-processed IN738LC experiences G values of approximately 0.2×10^7–7×10^7 K m^{-1} and R values of roughly 0.01–0.20 m s^{-1} across the melt pool, with high-G/low-R regions favouring columnar growth and lower-G/higher-R regions trending toward equiaxed growth [98]. These reported ranges reflect alloy-specific G–R trajectories rather than a broadly transferable critical G/R threshold.

Processing parameters influence CET primarily by modifying these local solidification conditions. Short-vector scanning, localised melt-scan patterns, and periodic scan rotation

continuously redirect heat flow and interrupt epitaxial growth, increasing opportunities for equiaxed nucleation [74,77,84,99]. Hatch spacing and layer thickness similarly modify melt-pool overlap and thermal gradients; excessive overlap tends to preserve directional heat flow, whereas controlled changes in melt-pool geometry can disrupt epitaxial continuity and promote grain refinement [13,73,100]. Thus, scanning parameters should be interpreted as controlling both the thermal field and the kinetic conditions for nucleation rather than as simple modifiers of G/R.

The resulting CET response is strongly alloy dependent. In IN718, rapid solidification promotes Nb- and Mo-associated enrichment of the interdendritic liquid, modifies constitutional supercooling and the local solidification path, and favours Nb-rich non-equilibrium constituents, such as the Laves phase [65,101,102]. IN738/IN738LC differs because its γ'-forming chemistry and segregation behaviour produce a distinct local phase-selection response and a comparatively restricted LPBF processing window [28,45,67,68]. Consequently, growth restriction and effective freezing behaviour cannot be inferred from G/R alone; they emerge from the combined effects of thermal conditions, solute partitioning, interface kinetics, and non-equilibrium phase stability. This explains why IN718 and IN738 can exhibit different CET responses even under comparable nominal thermal conditions.

In practical terms, IN625 shows considerable susceptibility to grain-structure modification through scanning and thermal perturbation [73,80,82], while IN718 grain refinement depends additionally on its segregation-sensitive solidification behaviour [65,74,77,84]. IN738/IN738LC retains a stronger tendency towards columnar growth and cracking, although targeted scanning strategies can interrupt grain continuity and promote refinement [75,87,88,91]. These differences demonstrate that CET should be treated as an alloy-specific competition between epitaxial growth and nucleation rather than as a universal G/R-controlled transition.

Microsegregation further connects solidification with subsequent thermal evolution. In IN718, Nb/Mo enrichment promotes interdendritic Laves formation, whereas IN738/IN738LC exhibits distinct carbide and γ' evolution during and after rapid solidification [65,89,101–105]. However, these phases should not be assigned an equivalent grain-boundary-pinning role. For LPBF IN738LC, Hu et al. [105] attributed impeded grain-boundary migration during subsequent thermal treatment primarily to carbide-particle pinning and solute segregation, while rapid LPBF cooling restricted γ' nucleation and growth. Therefore, current evidence supports an alloy-dependent coupling between segregation, secondary-phase evolution, and grain-boundary mobility, but does not establish a universal Laves/γ'-mediated pinning mechanism during multi-layer LPBF thermal cycling. Table 4 provides an overview of how cooling rate affects grain size and grain morphology in LPBF-fabricated IN625, IN718, and IN738 alloys.

Table 4. Relationship between cooling rate, grain size, and grain morphology in LPBF-processed Inconel alloys (IN718, IN625, and IN738).

Ref	Alloy	Cooling Rate (K/s)	Grain Size (μm)	Grain Type	Key Observation
Zhu et al. (2023) [106]	IN625	~10^6 (high)	Without Layer Thickness Variation (LTV) (~50–75 μm) With Layer Thickness Variation (LTV)-(~30–55 μm)	Without LTV-coarse columnar With LTV-equiaxed	Changes in the temperature gradients induced by LTV suppress the formation of columnar grains. This results in a 30% reduction in grain size and a more uniform structure.

Table 4. *Cont.*

Ref	Alloy	Cooling Rate (K/s)	Grain Size (μm)	Grain Type	Key Observation
X. Zhang et al. (2025) [80]	IN625	Very high ($\sim10^5$–10^7)	XY plane: ~53 μm XZ/YZ plane: ~107 μm	Columnar + equiaxed (heterogeneous microstructure)	LPBF Inconel 625 has a heterogeneous microstructure characterised by columnar and equiaxed grains, wherein elevated cooling rates result in anisotropic grain dimensions, and deformation facilitates grain refinement via slip, twinning, and shear banding.
K. Gruber et al. (2024) [86]	IN718	$\sim10^5$–10^6	Grain size (as-built): ~23–26 μm (number-based) ~100–200 μm (area-based).	Columnar dendritic grains	Suppression of grain expansion enhances strength.
A. Tajyar et al. (2022) [107]	IN718	$\sim10^5$–10^7	~27 μm (X–Y) and ~46 μm (X–Z) in as-built condition. After heat treatment → grain coarsening (up to ~274 μm)	Columnar dendritic grains (as-built) Equiaxed grains after heat treatment	Rapid solidification in LPBF yields columnar-dendritic grains that subsequently evolve into coarse-equiaxed grains following heat treatment, attributed to recrystallisation and grain growth.
Cloots et al. (2016) [67]	IN738	High cooling rate ($\sim10^4$–10^6)	~600–700 μm (length)	Columnar	Robust columnar-grain development in the build direction, resulting from directional solidification
J. Xu et al. (2023) [9]	IN738	High cooling rate ($\sim10^4$–10^6)	~11–35 (width)	Equiaxed/columnar	Transformation from columnar to equiaxed grains during hot isostatic pressing

Overall, CET in LPBF Inconel alloys results from the coupled effects of G and R, nucleation undercooling, constitutional supercooling, solute redistribution, and interface kinetics rather than from G/R alone. The available evidence therefore supports alloy-specific CET regions in the G–R space rather than a universal critical ratio, with the transition determined by competition between the imposed thermal field and composition-dependent nucleation/growth restriction. Accordingly, CET optimisation requires simultaneous control of the thermal field and alloy-specific solidification response, providing a more physically meaningful basis for reducing texture, anisotropy, and cracking susceptibility [72,75,77,88,96–98].

4.3. Texture and Anisotropy

The crystallographic texture in LPBF originates directly from directional solidification and epitaxial grain growth, which are among the main factors driving the anisotropic mechanical response of nickel-based superalloys. Unlike conventional manufacturing processes, LPBF exposes the molten material to multiple thermal cycles and highly directional heat removal, resulting in grains that preferentially grow in the build direction. Favourably oriented grains with respect to this heat flow form a layer-by-layer arrangement ahead of their neighbours, resulting in a strong fibre texture that controls material deformation, the development of residual stresses, and the final fracture path [78–81]. Texture formation is primarily governed by the interactions among the thermal gradient, the solidification direction, and competing dendritic growth. Since solidification is fast, dendrites tend to grow in the direction opposite to heat extraction, i.e., generally parallel to the build axis. In FCC nickel superalloys, this competitive growth process favours a dominant ⟨001⟩ fibre texture, as grains with this orientation grow fastest during directional solidification. The preference is further enhanced by epitaxial selection during layer-by-layer deposition, leading to long columnar grains that can span several layers [78,79].

The fundamental mechanism of texture development is common across Inconel alloys processed by LPBF, but the intensity of the resulting texture depends on alloy compo-

sition, process parameters, and scanning strategy. Under normal scanning conditions, sustained directional heat flow promotes the formation of a strong ⟨001⟩ texture in Inconel 625 due to the potential for stable epitaxial growth. However, scan rotation or hybrid scanning approaches periodically disturb the thermal field and interfere with competitive grain growth, thereby weakening the texture and resulting in finer grains with less anisotropy [80–82]. Inconel 718 exhibits a similar trend during repeated thermal cycling, resulting in strong columnar growth in the build direction. However, the degree of texture formation depends strongly on scan rotation, hatch spacing, and the extent of melt-pool overlap. The layer-rotation schemes of 67° or 90° break the directional heat flow, reduce the grain aspect ratio, and lead to a more varied distribution of crystallographic orientations. The effect of rotated scanning in reducing texture intensity, increasing grain-orientation randomness, and decreasing mechanical anisotropy has been repeatedly confirmed by EBSD studies [74,78,79,84,85]. Among the three alloys, Inconel 738 usually has the strongest texture because of its narrow processing window and high γ' fraction, both of which favour continued epitaxial growth under steep thermal gradients. This results in a strong orientation dependence of the alloy deformation behaviour and a higher susceptibility to solidification cracking. More recent work shows that altering the scan strategy and thermal history can partially suppress this preferred orientation, improve texture and cracking resistance, while maintaining high-temperature mechanical properties [75,88–91,99]. Figure 5 shows EBSD orientation maps and inverse pole figures that document changes in preferred grain orientation under various processing conditions, illustrating the impact of build orientation and scan strategy on crystallographic texture [78].

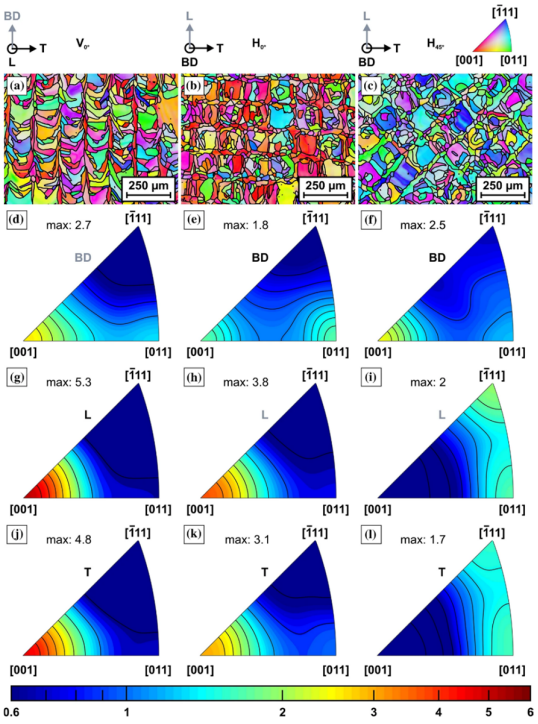


Figure 5. Orientation maps (**a**–**c**) together with logarithmically scaled inverse pole figures (**d**–**l**) are shown for sections V0° BD–T (**d**,**g**,**j**), H0° L–T (**e**,**h**,**k**), and H45° L–T (**f**,**i**,**l**). Grey arrows on the orientation maps denote loading directions, while the inverse pole figures capture the corresponding crystallographic texture intensity (m.r.d.). Taken together, the figure illustrates how different scan strategies alter grain orientation and texture evolution, leading to variations in crystallographic anisotropy that, in turn, shape the mechanical response of LPBF-fabricated Inconel alloys [78].

Figure 6 shows further details of the local deformation behaviour. Kernel Average Misorientation and Geometrically Necessary Dislocation analyses show the strong influ-

ence of local grain orientation on strain localisation, fracture initiation, and toughness anisotropy. Taken together, these results imply that crystallographic texture controls the distribution of plastic deformation under mechanical loading and the grain orientation [108]. Figure 7 provides a summary of the overall mechanism linking directional solidification, epitaxial growth, texture, and anisotropic mechanical behaviour of LPBF-fabricated Inconel 625, 718, and 738. The key texture characteristics of the three alloys are compared in Table 5.

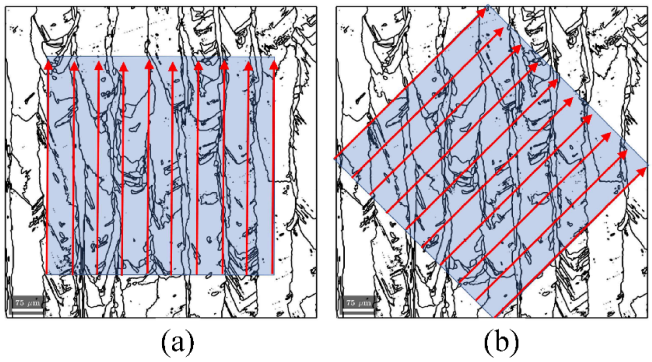


Figure 6. Approach used to extract Kernel Average Misorientation (KAM) and Geometrically Necessary Dislocation (GND) profiles across the grain structure. Within a 550 × 550 μm region, ten analytical lines were laid out: (**a**) vertical lines (0°) within a horizontal reference frame for R0-0 specimens, and (**b**) diagonal lines (45°) within a rotational reference frame for R0-45 specimens. This approach allows for systematic quantification of orientation-dependent strain localisation and dislocation density, thereby clarifying the relationship between scan strategy, microstructural heterogeneity, and the deformation behaviour of LPBF-fabricated Inconel alloys [108].

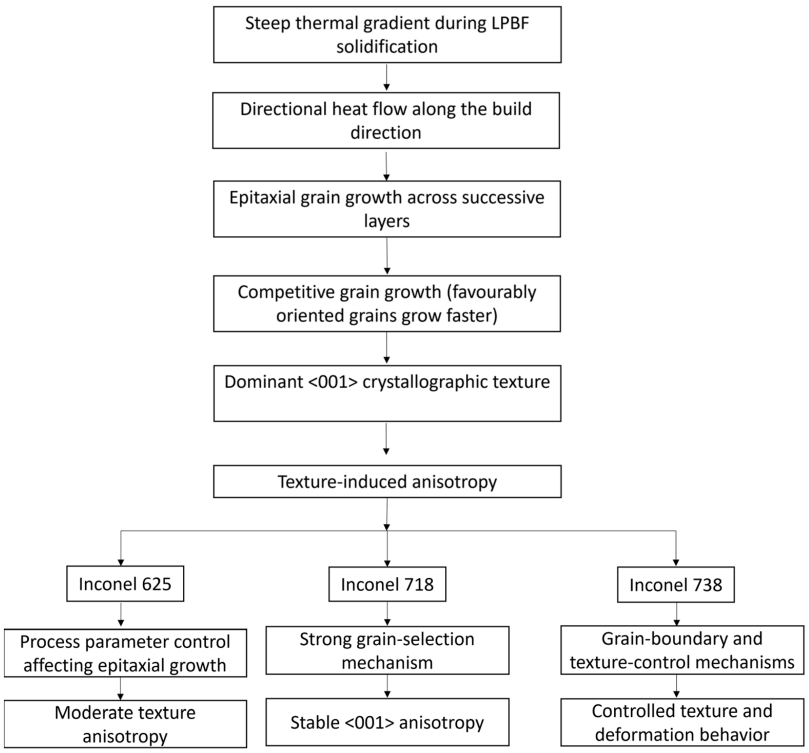


Figure 7. Mechanism of texture-induced anisotropy for Inconel 625, Inconel 718, and Inconel 738 alloys [46,78–81,90,91,106,108–110].

Table 5. Key insights of texture and anisotropy in grain structure evolution.

Alloy	Dominant Texture Orientation	Grain-Growth Mechanism	Cause of Texture Formation	Resulting Anisotropy
Inconel 625	Strong <001> texture along the build direction	Epitaxial grain growth across layers with competitive grain selection	Directional solidification driven by steep thermal gradients in LPBF; process parameters (e.g., layer thickness variation) can disrupt epitaxy	Direction-dependent tensile strength and ductility, especially at elevated temperatures
Inconel 718	Pronounced <001> columnar texture parallel to the build direction	Competitive grain growth during layer-by-layer solidification	Thermal gradient-driven epitaxial growth favours <001>-oriented grains; texture evolution influences slip activation	Micromechanical anisotropy and orientation-dependent fracture toughness
Inconel 738 (IN738LC)	Dominant <001> columnar grains aligned with thermal gradient	Competitive grain growth with texture-control mechanisms	Strong directional heat flow during LPBF promotes epitaxial growth; grain selection modifies crystallographic texture	Orientation-dependent deformation behaviour and high-temperature mechanical anisotropy

Overall, the literature consistently indicates that directional solidification and competitive epitaxial growth cause the crystallographic texture in LPBF. The degree of preferred orientation differs among Inconel 625, 718, and 738 due to differences in composition and thermal response, but the formation mechanism is fundamentally the same in all three systems [78–81,90,91,108–110]. Crystallographic texture bridges the gap between grain morphology and mechanical behaviour in the process–structure–property paradigm. Strong columnar textures result in increased directional strength but at the cost of increased anisotropy, localised residual stress, and orientation-dependent fracture tendencies, while suppression of the preferred texture by tailored processing favours more isotropic properties and enhanced structural reliability. Texture control is thus a key lever to improve the fatigue resistance, fracture toughness, and high-temperature performance of LPBF-fabricated Inconel parts [78,79,81,90,91,108–110].

In addition to their effects on mechanical behaviour, grain morphology and crystallographic texture also play a fundamental role in the evolution of defects during LPBF. Grain orientation, grain boundary properties, and local solidification conditions are directly responsible for the susceptibility to solidification cracking, porosity formation, and residual stress development by controlling melt-pool stability and strain accommodation during rapid solidification. Therefore, understanding the correlation between grain evolution and defect formation is essential for establishing robust process–structure–property relationships and enabling reliable LPBF processing of Inconel alloys. The next section discusses mechanisms of defect formation and process stability [75,85,87–89,91,99].

5. Defect Formation and Process Stability

5.1. Insufficient Energy Input

One of the major causes of process instability in LPBF is insufficient energy input, which directly results in lack-of-fusion (LOF) defects and broken melt tracks. This is because when the laser power is low, the scanning speed is high, the hatch spacing is wide, or the powder layer is thick, the energy actually delivered to the powder bed is insufficient; the powder particles are not sufficiently melted, and the previously deposited layer is not sufficiently remelted. Then, adjacent tracks fail to overlap properly, resulting in irregular melt-pool shapes and poor metallurgical bonding between layers [36,50]. From the melt-pool side, the thermal energy limits how far the liquid metal can flow and how well it can wet the surrounding powder. Instead of a continuous track, melting occurs only in isolated patches, leaving unmelted particles and unbonded zones scattered throughout

the build. These gaps prevent epitaxial grain growth across layers and produce irregular pore networks that are far more detrimental than isolated gas pores. LOF defects have sharp, irregular edges that result in high stress concentrations under load and are among the most damaging defect types to structural performance [36,50,69].

Low energy input can also cause balling, in which the melt breaks up into isolated spherical droplets rather than forming a continuous track. This is because, at high scan speeds, the poor wetting and capillary instability of the melt pool are exacerbated, reducing the duration of laser–powder interaction. Broken tracks lead to weakened interlayer bonding and increased local porosity, which destabilise the deposition of subsequent layers and contribute to defect buildup throughout the build [111]. LOF defects are common in LPBF processed Ni-based superalloys, but the mode of appearance varies with different alloys. Inconel 625 is a generally weld friendly and crack resistant material, such that moderate variations in process parameters will not cause significant structural damage. In contrast, Inconel 718 is more sensitive to energy input, as partial melting can lead to increased elemental segregation and to Nb-rich interdendritic regions during solidification. Inconel 738 is already less processable due to its high γ' fraction, but under insufficient melting, it becomes even more microstructurally heterogeneous, creating sites where cracks can later initiate [36,45,65,69].

5.2. Significant Energy Input

Where too little energy prevents complete melting, too much energy leads to a different kind of instability associated with keyhole-mode melting. High laser power, low scan speed, or high volumetric energy density causes the melt-pool temperature to rise rapidly, leading to rapid metal vaporisation and strong recoil pressure at the liquid–vapour boundary. Under these conditions, the melt pool transitions from a shallow, conduction-mode shape to a deep, narrow vapour cavity—the keyhole. A stable keyhole can improve laser energy absorption, but heavy vaporisation tends to destabilise the cavity, leading to continuous oscillation. The competition between surface tension, Marangoni convection, recoil pressure, and vapour fluctuations defines stability. If the cavity closes before the trapped vapour can escape, spherical pores are trapped within the solidifying melt, a signature of keyhole porosity. These pores are smooth and roughly spherical, unlike the jagged shapes typical of LOF defects, because they originate from trapped vapour bubbles rather than incomplete melting [111,112].

Real-time melt-pool monitoring has also demonstrated that excessive energy input leads to increased spatter and melt-pool fluctuations, both of which reduce process stability. Molten particles ejected from the melt pool can fall back onto the powder bed, disrupting powder spreading and the absorption of subsequent laser passes. This additional unevenness of the thermal field increases the possibility of porosity formation in subsequent layers [113]. In addition, the solidification behaviour and chemistry of each alloy also determine its sensitivity to excess energy. In general, Inconel 625 has a larger process window due to its good weldability and reduced risk of cracking. Nb segregation to interdendritic liquid can promote the formation of brittle Laves phases upon solidification, making Inconel 718 more susceptible to localised overheating problems. Inconel 738 is the most prone to excessive thermal input due to its high γ' strengthening fraction and complex solidification behaviour, meaning that segregation-driven cracking is much more likely to occur when melt-pool conditions are close to instability [45,65,69,103]. Thus, the process needs to remain in the conduction mode to ensure stable LPBF builds rather than drift into unstable keyhole mode. The right combination of laser power, scan speed, hatch spacing, and layer thickness not only limits porosity but also reduces melt-pool oscillation,

reduces spatter, and improves overall stability, setting up favourable conditions for the microstructure that develops afterwards [36,50,111–113].

5.3. Defect Formation Mechanisms

5.3.1. Gas Entrapment and Powder-Related Effects

Aside from energy input, gas entrapment and powder quality are also important factors in defect formation in LPBF [50,113]. Gas porosity is mainly caused by trapped shielding gas, gas trapped in atomised powder particles and poor gas escape due to unstable melt-pool behaviour during fast solidification. Characteristics of the powder, such as particle size distribution, morphology, oxidation state, moisture uptake, and recycling history, influence powder packing density, laser absorptivity, and melt-pool stability. Excessive spattering has also been shown to hinder powder spreading and to induce local thermal inhomogeneities that favour pore formation and surface defects [113]. Although gas porosity is generally less detrimental than lack-of-fusion defects, an excess of pores still degrades process consistency and causes localised microstructural heterogeneity under unstable processing conditions.

5.3.2. Rapid Solidification and Alloy Segregation

Rapid solidification is an intrinsic property of LPBF and has a twofold effect. It refines the microstructure on one side and causes elemental segregation under non-equilibrium conditions on the other. The fast-cooling rate gives little time for diffusion, trapping the alloying elements in the remaining interdendritic liquid and creating localised chemical inhomogeneity that can encourage brittle-phase formation and cracking during solidification [36,65]. The extent of segregation is strongly dependent on the alloy's chemistry. Inconel 625 is characterised by the segregation of Nb and Mo mainly, and is relatively resistant to cracking. Inconel 718 is susceptible to the formation of Nb-rich Laves phases, which deteriorate local ductility [36,50,65].

The rapid thermal cycling inherent to LPBF can suppress the formation of the primary strengthening γ'' (Ni_3Nb) phase, along with secondary γ' [Ni_3(Al,Ti)] precipitates, in the as-built condition, leaving a supersaturated γ matrix, while Nb partitioning toward cellular and interdendritic regions encourages localised Laves-phase development. Subsequent layer-wise thermal exposure, and particularly post-build ageing, supplies the time-temperature conditions necessary for γ''/γ' precipitation to proceed. As a result, the ultimate strengthening behaviour of LPBF-processed IN718 depends not only on the nominal alloy composition but also on the non-equilibrium Nb distribution inherited from rapid solidification, since Nb tied up in interdendritic Laves constituents becomes unavailable for later γ'' precipitation [114].

In contrast, Inconel 738 exhibits substantially greater cracking susceptibility due to its γ'-strengthened microstructure and complex segregation behaviour. For IN738, however, segregation alone does not explain crack initiation. Solute enrichment can depress the local solidus and prolong the persistence of interdendritic or grain-boundary liquid films, creating a mechanically weak region during the final stages of solidification or subsequent reheating. Cracking becomes critical when this vulnerable liquid state coincides with transient tensile stress/strain generated by constrained thermal contraction during rapid heating and cooling. Thus, crack susceptibility is governed by the temporal overlap between liquid-film persistence and thermo-mechanical loading rather than by thermal gradients or segregation independently. This coupling distinguishes two cracking mechanisms in IN738. Solidification cracking occurs within the solidifying melt pool or mushy region when persistent interdendritic liquid films cannot accommodate the tensile strain generated during terminal solidification.

In contrast, liquation cracking occurs in the reheated heat-affected region, where local grain-boundary liquation creates mechanically weak intergranular regions that can separate under transient tensile loading. Grain-boundary character and crystallographic misorientation may further influence liquid-film continuity and strain accommodation, thereby modifying crack susceptibility. Consequently, cracking should be interpreted as the coupled outcome of alloy-specific segregation and solidification, liquid-film persistence, grain-boundary characteristics, and transient thermo-mechanical loading rather than any single processing parameter [45,69,103]. The primary mechanisms of defect production, the process conditions controlling them, the defects they cause and the microstructural properties observed for Inconel alloys manufactured by LPBF are summarised in Table 6.

Table 6. Physics-based classification of defect formation mechanisms during LPBF.

Physical Mechanism	Primary Process Conditions	Typical Defects	Characteristics	References
Insufficient energy input	Low laser power, high scan speed, large hatch spacing	Lack of fusion, balling	Incomplete melting, discontinuous melt tracks	[36,50,69]
Excessive energy input	High laser power, low scan speed, excessive VED	Keyhole porosity	Vapour cavity instability and pore entrapment	[111,112]
Gas entrapment and powder-related effects	Powder contamination, shielding gas, recycled powder	Gas porosity, inclusions, spatter-induced defects	Trapped gas, oxide inclusions and local heterogeneity	[50,113]
Rapid solidification and alloy segregation	High cooling rates, steep thermal gradients, and alloy chemistry	Microsegregation, solidification cracking	Interdendritic segregation and grain-boundary embrittlement	[36,45,65,69,103]

5.3.3. Coupled Defect Evolution and Failure Pathways

Defects in LPBF are not independent outcomes, as melt-pool instability, metallurgical heterogeneity, and thermo-mechanical loading interact to produce sequential-failure pathways. Keyhole instability and collapse drive pore entrapment [111,112], while insufficient melting produces irregular, unbonded regions due to lack of fusion [36,50,69]. These discontinuities act as local stress-concentration sites, increasing the susceptibility to crack initiation when combined with residual tensile stresses or embrittled grain boundaries. Defect evolution is therefore represented as a coupled sequence: process instability → primary defect → local stress/metallurgical concentration → cracking and property degradation, rather than as isolated defect categories.

Powder-related effects provide a second coupling pathway. Recycled or contaminated powder promotes gas porosity, oxide inclusions, and local chemical heterogeneity [50,113], which interact with segregation-sensitive grain boundaries and transient thermal stresses. This interaction is more critical in IN718 and particularly IN738/IN738LC, where interdendritic segregation and grain-boundary embrittlement already increase cracking susceptibility [36,45,65,69,103]. Porosity, lack of fusion, inclusions, segregation, and residual stress are therefore interacting contributors to crack initiation and mechanical degradation rather than mutually independent defects. This coupled-defect interpretation is incorporated into the PSPC framework to connect upstream melt-pool and solidification instabilities with downstream failure behaviour.

5.4. Specific Defect Behaviour of Inconel

The fundamental mechanisms of defect generation are similar to those of general Ni-based superalloys processed by LPBF, but the susceptibility of each alloy to specific types of defects is highly dependent on the chemistry, solidification behaviour, and precipitation characteristics. These alloy-to-alloy differences influence the processing window, melt-pool stability, and defect tolerance of each alloy during fabrication. Of these three, Inconel 625 has the widest processing window due to its good weldability and relatively low γ' strengthening fraction, which makes it fairly immune to solidification cracking even in the presence of Nb- and Mo-rich interdendritic segregation at rapid solidification [36,50]. Inconel 718 is more sensitive to thermal fluctuations because Nb segregation and Laves-phase formation reduce local ductility [65].

IN738 represents the most crack-sensitive case because segregation-sensitive solidification interacts with the transient thermal stresses generated during LPBF [45,69,103]. Importantly, its cracking response should not be treated as a single generic hot-cracking mechanism. Solidification cracking develops during the final stage of melt-pool solidification, when solute-enriched interdendritic liquid persists while thermal contraction imposes tensile strain on the mechanically vulnerable mushy region. In contrast, liquation cracking occurs after nominal solidification in the reheated heat-affected region, where segregated low-melting constituents or grain-boundary regions locally remelt, forming liquid films that can separate under thermal stress. These mechanisms and their distinct locations are directly reported for IN738/IN738LC. Grain-boundary crystallography further modifies this susceptibility. LPBF IN738LC has been reported to exhibit preferential cracking along grain boundaries with high misorientation angles, indicating that grain-boundary character influences the ability of liquid-containing boundaries to accommodate the imposed strain [115]. Thus, the high cracking tendency of IN738 is better explained by the coupled interactions of segregation, liquid-film persistence, grain-boundary character, and transient thermo-mechanical loading rather than by alloy chemistry or thermal gradients alone.

Such differences show that alloy chemistry is as important as process parameters in determining defect evolution during LPBF. Stable processing conditions reduce defects across all three alloys, but the acceptable processing window narrows from Inconel 625 to Inconel 718 and IN738 as segregation and cracking susceptibility increase. For IN738, optimisation must therefore control not only melt-pool stability but also the metallurgical and thermo-mechanical conditions under which liquid-containing boundaries are subjected to tensile loading. This interpretation is consistent with experimental LPBF IN738LC results showing that both residual stress and melt solidification time influence crack density [70]. Table 7 summarises the alloy-specific factors affecting defect generation and process stability.

Table 7. Comparative study on the defect susceptibility and process stability of LPBF fabricated Inconel alloys.

Alloy	Dominant Metallurgical Characteristics	Primary Defect Susceptibility	Relative Process Stability
Inconel 625	Good weldability; Nb and Mo segregation	Lack of fusion and gas porosity under inadequate processing conditions	High
Inconel 718	Nb segregation and Laves phase formation	Segregation-induced defects and porosity	Moderate
Inconel 738	High γ' content; complex solidification	Solidification cracking and grain-boundary embrittlement	Low

While understanding the mechanisms of defect formation is important in itself, effective LPBF processing requires defect-specific mitigation techniques. As different defects arise from distinct thermal and metallurgical instabilities, it is not possible to expect a single optimisation approach to eliminate all defect types simultaneously. The choice among optimising process parameters, thermal management, controlling powder quality, modifying the scan strategy, and post-processing treatments should be made based on the defect mechanism that dominates the given case. Table 8 summarises the main approaches to defect mitigation and their effects on process stability and component quality [36,50,65,103,111–113].

Table 8. Comparison of defect mitigation techniques for LPBF-fabricated Inconel alloys.

Defect Type	Primary Cause	Recommended Mitigation Strategy	Expected Outcome	Representative References
Lack-of-fusion (LOF)	Inadequate energy input, weak melt-track overlap, overly wide hatch spacing	Raise the laser power, lower the scan speed, and fine-tune the hatch spacing and layer thickness	Better densification, stronger interlayer bonding, and less LOF-related porosity	[36,50,69]
Balling	Elevated scan speed, inadequate wetting, and capillary instability	Fine-tune scan speed, enhance powder spreading, and sustain a stable melt-pool geometry	Continuous melt tracks, lower surface roughness and porosity	[111,113]
Keyhole porosity	Excessive laser-energy density, unstable vapour cavity	Lower VED, fine-tune laser power and scan speed, apply beam shaping	Stable conduction-mode melting, reduced keyhole porosity	[111,112]
Gas porosity	Trapped shielding gas, powder contamination, and reuse of recycled powder	Employ high-quality powder, sustain an inert atmosphere, dry powder, and control recycling	Fewer pores, improved fatigue resistance, and greater process consistency	[50,113]
Solidification cracking	Steep thermal gradients, alloy segregation, high γ' content	Preheat the substrate, optimise scan strategy, refine grain structure, modify alloy composition	Lower cracking susceptibility, improved structural reliability	[45,65,69,103]
Microsegregation	Rapid solidification coupled with limited elemental diffusion	Optimise thermal history, apply suitable post-build heat treatment	Reduced segregation, improved phase homogeneity and mechanical performance	[36,65,103]
Residual stress and distortion	Rapid heating-cooling cycles and steep thermal gradients	Preheat the baseplate, optimise scan strategy, and apply stress-relief heat treatment	Reduced distortion, lower residual stress, improved dimensional accuracy	[24,25,116,117]

In general, defect formation in LPBF is a consequence of the interplay among process parameters, melt-pool stability, rapid solidification, and alloy chemistry. Therefore, it is important to maintain the melt pool in a stable conduction mode and to select processing conditions appropriate to the alloy to minimise defects and maintain a stable process. Although processing is the source of defects, its influence extends beyond the manufacturing stage, affecting the microstructure's development and, hence, the material's mechanical properties. The links are the process–structure–property relations discussed in the next section.

6. Process–Structure–Property Relationships

6.1. Integrated Process–Structure–Property–Control Framework

As discussed in the previous sections, the performance of LPBF Inconel components cannot be attributed to a single processing parameter or a single microstructural feature. Instead, the final component performance results from coupled interactions among processing conditions, thermal history, microstructural development, defect formation, and post-processing strategies. This integrated PSPC relationship provides a holistic view of how the changes introduced during fabrication are transferred through the material to

determine its final mechanical behaviour. Therefore, LPBF optimisation is a multi-variable problem, and the interdependence of the variables should be handled simultaneously rather than tuning the parameters one by one.

The thermal history of the material in the LPBF process is governed by laser power, scan speed, hatch spacing, layer thickness, powder characteristics, and scan strategy. Although these parameters do not directly affect the final properties, they do affect melt-pool stability, the temperature gradient, the cooling rate, and the solidification kinetics. These thermal conditions then govern grain morphology, crystallographic texture, elemental segregation, precipitate evolution, defect formation and the build-up of residual stress. These structural features, together, in turn, control the strength, hardness, ductility, fatigue resistance, creep behaviour, and high-temperature performance of the produced Inconel parts. Therefore, the process–structure–property relationship is more a continuous hierarchical path than a chain of independent, disconnected events [101,102,104].

This underlying PSP relationship is common to Inconel 625, Inconel 718, and Inconel 738, but the chemistry of each alloy changes at each stage of the framework in different ways. Inconel 625 has relatively good weldability and a wider processing window, resulting in a stable melt-pool behaviour over a wider range of conditions. Inconel 718 is more sensitive to thermal history, as Nb segregation and the resulting gamma-prime/gamma-double-prime precipitation strongly influence the final mechanical properties. The processing window for Inconel 738 is even narrower due to its high γ' volume fraction and greater susceptibility to solidification cracking. This means that the same LPBF processing conditions can result in different microstructures and mechanical responses depending on the alloy, highlighting the need for an alloy-specific process optimisation [101,102,104,105,118–121].

Another important part of the PSP framework is the feedback loop between process control and post-processing. In contrast to traditional manufacturing methods, the LPBF process enables gradual improvement in material performance by adjusting process parameters, scan strategies, heat treatment, hot isostatic pressing (HIP), remelting, and surface engineering. These control strategies not only improve individual properties in isolation but also act on the underlying microstructure itself, reducing porosity, relieving residual stress, refining precipitate distribution, and improving microstructural stability. In this respect, process control serves as a feedback mechanism that continuously links manufacturing parameters to the desired structural features and ultimately component performance, closing the loop of the integrated process–structure–property–control cycle [101,122,123]. The proposed Central PSPC framework shown in Figure 8 captures the relationships between LPBF processing parameters, thermal history, microstructural development, defect formation, mechanical behaviour, and optimisation strategies.

The PSPC framework describes the hierarchical relationships that govern LPBF, but the individual microstructural features do not contribute equally to material performance. The influence of grain morphology, crystallographic texture, precipitate evolution, porosity, and residual stress on the individual mechanical properties is associated with specific strengthening and deformation mechanisms. Therefore, a comparative assessment of such structure–property relationships is crucial to understand the mechanical behaviour of LPBF-fabricated Inconel alloys.

6.2. Structure–Property Relationships

The mechanical properties of LPBF-processed Inconel alloys arise from an interplay among grain morphology, crystallographic texture, precipitate evolution, defect population, and residual stress, rather than a single microstructural feature. These structural features evolve simultaneously during LPBF under common thermal conditions, and they interplay to determine the final mechanical response. It is thus important to understand the individ-

ual contribution of each microstructural feature to optimise the trade-off among strength, ductility, fatigue resistance, and high-temperature performance.

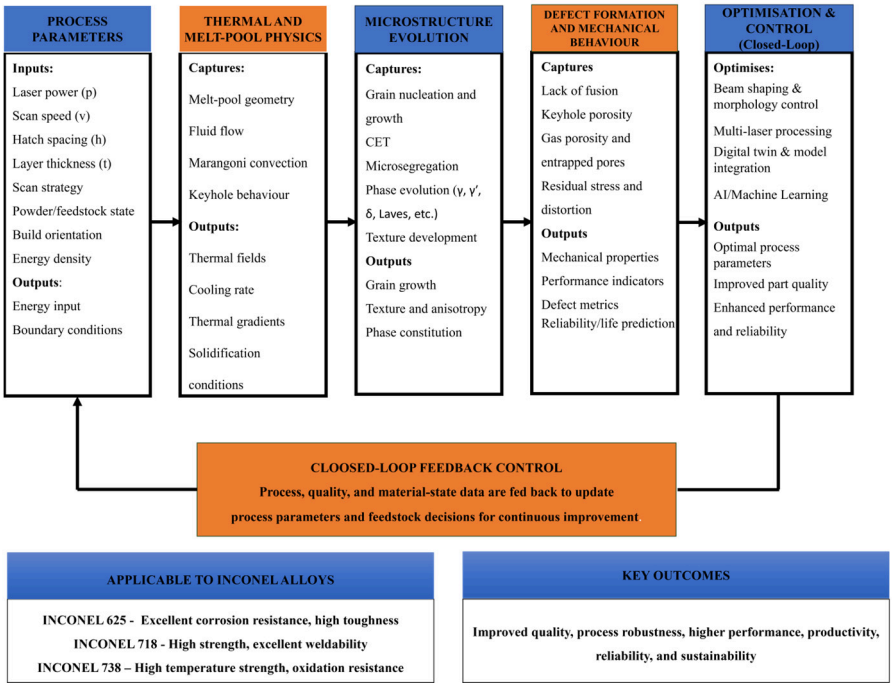


Figure 8. Integrated PSPC framework illustrating the relationships between LPBF processing parameters, thermal history, microstructural evolution, defect formation, mechanical properties, and optimisation strategies for Inconel 625, Inconel 718, and Inconel 738.

6.2.1. Grain Morphology and Strengthening Mechanisms

Grain morphology is one of the main factors controlling the mechanical behaviour of LPBF-fabricated Inconel alloys. Rapid solidification leads to fine cellular and cellular-dendritic structures with a higher grain boundary density, which blocks dislocation motion and increases yield strength through grain-boundary strengthening. The directional heat flow also promotes the growth of epitaxial columnar grains in the build direction, which leads to anisotropic mechanical behaviour. Thus, the overall mechanical response results from the competition between grain refinement and directional grain growth, rather than either alone [102,104,105,118–121].

The strengthening mechanism is active in all three alloys, but the dominant strengthening phases change with alloy chemistry. Most of the strength in Inconel 625 comes from grain refinement and solid-solution strengthening associated with cellular structures rich in Nb and Mo. Inconel 718, on the other hand, achieves substantially higher strength because grain refinement is assisted by precipitation strengthening from γ' and γ'' phases, particularly after appropriate heat treatment. In addition to carbide-reinforced grain boundaries, Inconel 738 is primarily strengthened by a large amount of γ' precipitates, which provide excellent high-temperature strength but poor processability during LPBF [104,118–121]. These observations indicate that grain refinement alone cannot account for the improved performance of LPBF-fabricated Inconel alloys. The mechanical strength arises from the interplay among grain morphology, precipitate strengthening, and alloy chemistry, underscoring the importance of integrated microstructural control during processing and post-processing.

6.2.2. Texture and Mechanical Anisotropy

LPBF is characterised by directional solidification, which promotes the formation of strong crystallographic textures that strongly influence the mechanical property anisotropy. Columnar grains oriented preferentially with the build direction provide efficient load paths under longitudinal loading, but typically exhibit reduced ductility and different deformation behaviour when loaded transverse to the build direction. As a consequence, the tensile strength, elongation, and fracture behaviour of LPBF components with the same composition may differ depending on the loading orientation [102,105,107,110,118].

The degree of anisotropy differs among the three alloys due to differences in solidification behaviour and post-processing response. The solidification behaviour of Inconel 625 is more stable and has a wider processing window, resulting in less anisotropy. The interaction between directional grain growth and precipitation hardening results in more pronounced orientation-dependent behaviour in Inconel 718, while Inconel 738 can retain significant anisotropy due to its coarse columnar grains and limited recrystallisation during processing. These results emphasise the importance of optimising scan strategies and heat treatment schedules to reduce anisotropy and achieve more uniform mechanical performance [102,105,106,119,121].

6.2.3. Porosity, Defects, and Tensile Properties

Although grain refinement and precipitation strengthening improve the mechanical performance, defects induced by processing are often the most limiting factor to structural reliability. Lack of fusion defects, keyhole porosity, and gas pores reduce the effective load bearing area and act as stress concentrators to accelerate the initiation of cracks under mechanical loading. Of these, irregularly shaped lack-of-fusion pores are the most detrimental to tensile properties, with their sharp geometry generating greater local stress concentrations than the more spherical gas pores [101,122,124–127].

The experimental work shows that tensile strength and ductility can be significantly improved by increasing component density through optimised parameter settings or remelting strategies. Considerable improvements in the mechanical properties of LPBF-processed Inconel alloys have been observed at relative densities above ~99.5%, underscoring the importance of porosity control. But the sensitivity to defects differs among the alloys. Inconel 625 shows relatively high ductility as long as porosity is low, while Inconel 718 is more susceptible to the combined effect of porosity and Nb-rich segregated areas. Inconel 738 is the most sensitive among the three, because pore defects tend to interact with grain boundary segregation and solidification cracking, resulting in faster fracture under tensile load [101,122,126,127]. The effect of defects is therefore more than a mere density reduction because their shape, distribution, and interaction with the surrounding microstructure together determine mechanical reliability. Thus, defect mitigation should be considered part of microstructural optimisation rather than a manufacturing target in itself. Table 9 summarises the relationships between the main microstructural characteristics and their effects on the mechanical behaviour of Inconel alloys produced by LPBF.

Table 9. Structure–property relationships in LPBF-fabricated Inconel alloys.

Microstructural Feature	Strengthening/Degradation Mechanism	Effect on Properties	Most Affected Alloy(s)	Key References
Fine cellular grains	Grain-boundary strengthening	Increase in Yield strength and hardness	625, 718	[118–120]
γ'/γ'' precipitates	Precipitation hardening	Increase in tensile strength and creep resistance	718, 738	[102,104,105,120,121]

Table 9. *Cont.*

Microstructural Feature	Strengthening/Degradation Mechanism	Effect on Properties	Most Affected Alloy(s)	Key References
Columnar grains and texture	Directional solidification	Increase in Strength and Anisotropy	718, 738	[102,104,105,121]
Porosity (LOF and gas pores)	Stress concentration	Decrease in Ductility and Fatigue life	All alloys	[101,122,124–127]
Residual stresses	Crack initiation	Increase in Fatigue resistance and Distortion	718, 738	[116,117,128]

The inherent microstructure provides the baseline mechanical response of LPBF-produced Inconel alloys, but final performance can be enhanced through suitable process control and post-processing. Techniques such as heat treatment, hot isostatic pressing (HIP), remelting, and surface engineering affect the basic microstructure, reduce defects and residual stress, and enhance long-term mechanical reliability. In the next section, we discuss these optimisation strategies.

6.3. Property Optimisation and Process Control

The mechanical properties of LPBF Inconel alloys can be further enhanced by combining process optimisation and post-processing strategies. The optimised laser parameters lead to stable melt-pool behaviour and limit defect formation during fabrication, while post-processing methods such as heat treatment, hot isostatic pressing (HIP), remelting, and surface engineering further enhance microstructural homogeneity by relieving residual stress, closing internal porosity, and controlling precipitate evolution [101,122,123]. These approaches utilise the intrinsic strengths of LPBF to enhance strength, fatigue resistance, and high-temperature performance.

The effectiveness of these optimisation strategies is alloy-chemistry-dependent. For Inconel 625, the heat treatment mainly serves to homogenise the microstructure and relieve stresses, whereas Inconel 718 can be strengthened considerably by precipitation of the γ' and γ'' phases, which also improve creep resistance. In comparison, optimisation of Inconel 738 involves controlling γ' precipitation, grain-boundary stability, and susceptibility to cracking, due to its narrow processing window [101,102,104,105,121,128]. In addition, recent progress in in situ monitoring and data-driven process control presents further opportunities to detect melt-pool instabilities and defect formation at an early stage, thereby improving process reliability and repeatability during LPBF fabrication [113,129]. The literature generally suggests that process optimisation and post-processing alone cannot lead to optimal mechanical performance. Instead, an integrated approach of stable LPBF processing with suitable post-processing treatments is key to producing dense, defect-minimised, and mechanically reliable Inconel components capable of meeting the demands of aerospace and high-temperature applications.

Based on the literature examined, it is concluded that the mechanical behaviour of LPBF-produced Inconel alloys depends on the coupled effects of process parameters, microstructure development, defect types, and post-processing, rather than on a single factor. Grain refinement, precipitation strengthening, and microstructural stability are beneficial for strength and high-temperature performance. However, structural integrity can be significantly compromised if defects, porosity, anisotropy, and residual stress are not adequately controlled. The comparison of Inconel 625, Inconel 718, and Inconel 738 further demonstrates that alloy chemistry heavily influences each alloy's re-

sponse to the same LPBF processing conditions, highlighting the need for alloy-specific optimisation strategies.

Significant progress has been made in establishing process–structure–property relationships through experimental work; however, the complex coupling between thermal history, melt-pool dynamics, microstructural evolution, and mechanical behaviour is difficult to capture solely through experimental approaches. This has led to an increasing importance of advanced modelling techniques to understand these multi-physics interactions, predict process outcomes, and accelerate process optimisation. The next section critically reviews the modelling approaches developed for simulating LPBF processing and discusses their capabilities, limitations, and prospects for Inconel alloys.

7. Critical Review of Modelling Approaches

7.1. Finite-Element Thermal Modelling

Numerical modelling based on the Finite-Element Method (FEM) remains the most popular approach for describing the thermal and thermomechanical response of LPBF, including the transient temperature distribution, melt-pool properties, residual-stress development, and part distortion. Most physics-based modelling frameworks developed for LPBF processing of Inconel 625, Inconel 718, and Inconel 738 [130–133] are based on the FEM, as the thermal history dictates the solidification pathways and the resulting microstructure. The FEM can quantitatively predict thermal gradients, cooling rates, and cyclic heating effects by introducing formulations of moving heat sources and physically representative boundary conditions, thereby supporting the development of process–structure–property relationships in nickel-based superalloys [130–132].

A systematic FEM-based framework for optimising the LPBF process is shown in Figure 9. The model uses key process parameters, such as laser power, scan speed, hatch spacing, and layer thickness, as inputs to predict melt-pool behaviour and the associated thermal history. The resulting simulation outputs are validated against experimental measurements and in situ monitoring data. Recent efforts have coupled FEM with machine-learning algorithms and digital twin architectures to improve predictive accuracy and computational efficiency across a wide range of manufacturing conditions [132,134].

Simulations of LPBF using FEM typically rely on a transient heat-conduction formulation, incorporating appropriate thermal boundary conditions, to capture how temperature evolves across the build. The predicted thermal fields, in turn, govern melt-pool dimensions, cooling rates, and thermal gradients, all of which have a direct bearing on solidification behaviour, the development of residual stress, and the extent of component distortion [130–133].

While FEM provides reliable thermal predictions, fully resolved simulations of entire LPBF parts remain computationally demanding, as the melt pool accounts for only a small portion of the overall computational domain. To overcome this constraint, multiscale FEM approaches employ a refined mesh near the moving melt pool and a coarser mesh elsewhere in the domain, thereby reducing computational expense while preserving predictive accuracy [133]. The thermal coupling between the global and local computational domains can be expressed as:

$$c^{+}\rho^{+}\frac{\partial T^{+}}{\partial t} - \nabla \cdot (k^{+}\nabla T^{+}) = Q + (k^{+} - k^{-})\frac{\partial T^{-}}{\partial n}, \tag{3}$$

$$c^{-}\rho^{-}\frac{\partial T^{-}}{\partial t} - \nabla \cdot (k^{-}\nabla T^{-}) = Q, \tag{4}$$

where T^{+} and T^{-} are the temperature fields of the global and local domains, respectively, while k^{+} and k^{-} denote the thermal conductivities associated with the corresponding

domains. This hierarchical approach allows for accurate resolution of local melt-pool dynamics while simultaneously capturing the overall thermal response of the component, making it well suited to industrial-scale LPBF simulation [133].

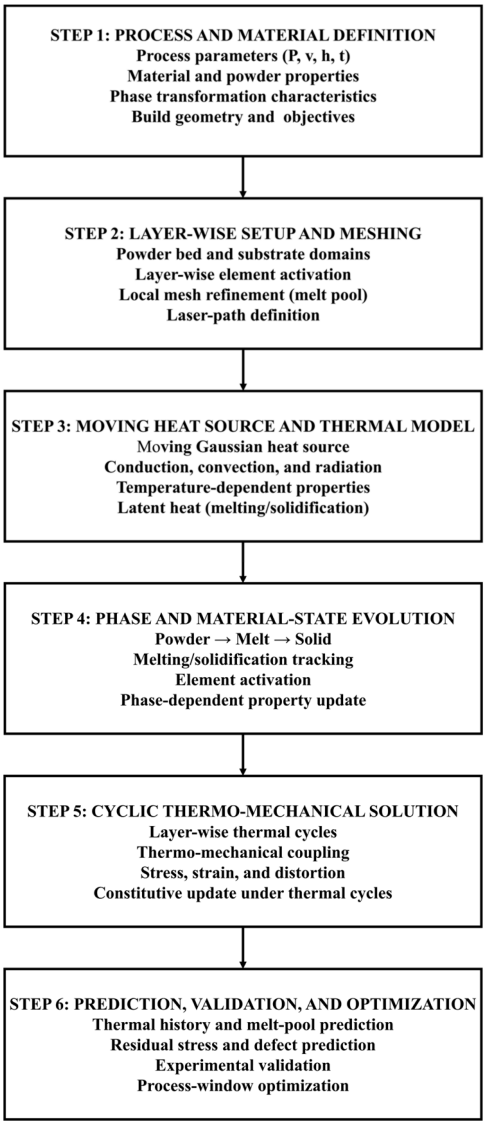


Figure 9. Systematic FEM framework of LPBF process optimisation.

Although widely adopted, standard FEM formulations do not explicitly account for melt-pool fluid dynamics, Marangoni convection, recoil pressure, or keyhole instability, all of which are critical in determining defect formation under high-energy-density conditions. Furthermore, since FEM provides thermal history but not a direct description of microstructural evolution, it is often coupled with phase-field, CALPHAD or cellular automata approaches to construct a more complete picture of process–structure–property relationships. As the mesh resolution increases and the component size grows, the computational demand increases as well, but recent coupling with reduced-order modelling, machine learning, and digital-twin frameworks has dramatically improved the computational efficiency and the predictive capacity of the models, thus allowing for real-time optimisation of the LPBF process [132–139]. However, the phenomena of grain nucleation, dendritic growth, and phase transformations during rapid solidification cannot be directly resolved by FEM alone. Therefore, phase-field and CALPHAD models are widely used to describe these mesoscale mechanisms and to establish quantitative relationships between

thermal history and resulting microstructural evolution in LPBF-processed nickel-based superalloys [94,95,134,135,140].

7.2. Phase-Field and CALPHAD Modelling

FEM provides reliable predictions of thermal history and cooling rates in LPBF, but it does not capture the microstructural evolution associated with rapid solidification. Properties that ultimately determine the mechanical performance of nickel-based superalloys are dendritic growth, competitive grain development, solute redistribution, and phase transformations; thus, mesoscale modelling is mandatory. Phase-field modelling combined with CALPHAD thermodynamics is one of the most powerful computational frameworks for describing the evolution of microstructure under the strongly non-equilibrium conditions typical of LPBF [94,95,134,135,140].

The phase-field variable evolves in time by minimising the system's total free energy.

$$\dot{\phi}_\alpha = \sum_{\beta \neq \alpha} M_{\alpha\beta} \left(\frac{\delta F}{\delta \phi_\alpha} - \frac{\delta F}{\delta \phi_\beta} \right), \tag{5}$$

where $M_{\alpha\beta}$ is the interface mobility, and F is the total free energy functional. This relation controls interface migration during solidification and allows prediction of dendritic growth, grain competition, and microstructural evolution during rapid solidification [94,95].

To capture microsegregation during rapid solidification, phase-field models incorporate solute transport through

$$\dot{c}_i = \nabla \sum_{\alpha=1}^{N} \sum_{j=1}^{k-1} \phi_\alpha D_{ij}^{\alpha} \nabla c_j^{\alpha}, \tag{6}$$

where D_{ij}^{α} is the diffusion coefficient of the component i in phase. These relations are useful for predicting microsegregation, elemental partitioning, and subsequent precipitation, which are of special interest for nickel-based superalloys, as segregation of Nb, Ti, and Mo strongly affects the formation of strengthening phases and cracking susceptibility [94,95].

The CALPHAD method provides a thermodynamic basis for describing how phase stability in multicomponent alloy systems depends on temperature and composition. Together with phase-field modelling, it enables the prediction of more physically realistic dendritic growth, γ/γ' evolution, Laves-phase formation, and microsegregation, thereby reinforcing the connection between thermal history and microstructural evolution in LPBF-processed Inconel alloys [94,95,135,140].

However, phase-field and CALPHAD models remain computationally expensive, as the motion of the solid-liquid interfaces must be accurately resolved, which requires fine spatial resolution and small time increments. Therefore, these models are usually applied in representative microscale regions driven by thermal histories from FEM, and hybrid multiscale frameworks combining FEM, phase-field, CALPHAD, and data-driven methods are continually improving computational efficiency while maintaining predictive accuracy [94,134,135,140].

7.3. Critical Comparison of Modelling Approaches

LPBF is characterised by strongly coupled thermal, fluid-flow, metallurgical and mechanical phenomena across several spatial and temporal scales. Consequently, a wide variety of computational modelling approaches have been employed to study different aspects of the process, including melt-pool behaviour and temperature evolution, as well as microstructure formation, residual-stress development, and mechanical performance. However, all the modelling techniques are tailored to a single physical phenomenon and have their own strengths and limitations. The choice of a suitable modelling ap-

proach depends on the prediction target, available computational resources, and the required level of physical fidelity. Therefore, a critical comparison of the existing modelling approaches is needed to clarify their applicability, limitations and directions for future development [95,130–137,140]. Tables 10 and 11 summarise their principal characteristics, predictive capabilities and engineering applications.

Table 10. Comparative analysis of the modelling methodologies used in the laser powder bed fusion of nickel-based superalloys [85,94,130–140].

Method	Main Strength	Main Limitation	Computational Cost	Best-Suited Application
FEM	Reliable prediction of temperature distribution, residual stress, and distortion	Does not explicitly account for melt-pool fluid flow or microstructural evolution	Medium–High	Predicting residual stress and distortion in Inconel 718 components
Computational Fluid Dynamics (CFD)	Resolves melt-pool flow dynamics, Marangoni convection, recoil pressure, and keyhole formation	Substantial computational demand with limited scalability	Very High	Modelling melt-pool dynamics and keyhole behaviour in Inconel 625
Phase-Field	Delivers high-fidelity prediction of dendritic growth and grain evolution	Computationally demanding and confined to microscale domains	Very High	Predicting solidification behaviour and grain morphology
CALPHAD	Provides an accurate prediction of phase stability and precipitation	Excludes spatial thermal gradients and melt-pool physics	Medium	Predicting phase evolution and precipitation
Cellular Automata (CA)	Enables efficient simulation of grain growth	Relies on simplified physical assumptions relative to phase-field models	Low	Predicting columnar-to-equiaxed grain transition
Machine Learning	Offers fast prediction of process–property relationships	Heavily dependent on the quality and availability of training data	Low (after training)	Process optimisation and defect prediction
Digital Twin	Combines modelling, monitoring, and adaptive process control	Implementation is complex, requiring robust data integration	High	Intelligent manufacturing and closed-loop process optimisation

Table 11. Comparative evaluation of the predictive capabilities of LPBF modelling approaches [85,94,130–140].

Method	Thermal Analysis	Melt-Pool Flow	Microstructure	Phase Evolution	Residual Stress	Real-Time Process Control
FEM	Excellent	Limited	Limited	Not Applicable	Excellent	Not Applicable
CFD	Good	Excellent	Limited	Not Applicable	Limited	Not Applicable
Phase-Field	Not Applicable	Not Applicable	Excellent	Good	Not Applicable	Not Applicable
CALPHAD	Not Applicable	Not Applicable	Good	Excellent	Not Applicable	Not Applicable
Cellular Automata	Not Applicable	Not Applicable	Good	Limited	Not Applicable	Not Applicable
Machine Learning	Moderate	Moderate	Moderate	Moderate	Moderate	Excellent
Digital Twin	Excellent	Excellent	Excellent	Excellent	Excellent	Excellent

Tables 10 and 11 indicate that a single modelling technique is not sufficient to capture the complexity of the LPBF process. FEM can reliably predict thermal history, residual stress, and distortion, but does not explicitly account for melt-pool hydrodynamics. In contrast, CFD can efficiently capture melt-pool flow, Marangoni convection, and keyhole behaviour, but its computational load limits its application for large-scale simulations [132,135,137]. Phase-field and CALPHAD models provide detailed insight into solidification, grain evolution, and phase transformations, but they are typically restricted to the microscale and

require thermal histories from FEM. However, cellular automata methods have increased computational efficiency at the expense of decreased physical fidelity. The complementary strengths and limitations have spurred an increasing interest in hybrid multiscale frameworks that couple multiple modelling strategies to achieve more comprehensive and predictive simulations of the LPBF process [95,134,135,140].

Current Challenges and Future Perspectives

One of the major challenges in LPBF modelling is the absence of reliable validation due to the experimental difficulty of measuring transient melt-pool behaviour, thermal gradients and rapid solidification. Most computational studies validate their predictions indirectly by comparing them with melt-pool dimensions, porosity measurements, residual-stress data, and post-build microstructural characterisation. Differences in the laser's absorptivity, powder morphology, temperature-dependent material properties, and boundary conditions also contribute to deviations between simulation results and experimental observations [130–133,135,137]. Another challenge is the lack of standardised benchmark problems and validation procedures. The wide range of process parameters, material systems, and experimental methods reported in the literature makes the direct comparison of different modelling approaches difficult. Shared validation protocols and publicly available benchmark datasets would help to build confidence in computational predictions and allow more consistent evaluation of emerging modelling strategies.

Although individual modelling techniques have made considerable progress, efficiently coupling thermal, fluid-flow, microstructural, and mechanical models remains a major challenge. Most existing frameworks are based on one-way coupling, in which the thermal histories computed by the FEM are passed to phase-field or CALPHAD simulations without feedback from the evolving microstructure or material properties [135,137,140]. Differences in spatial and temporal resolution only increase computational overhead, underscoring the need for more efficient multiphysics coupling strategies that can link melt-pool dynamics, solidification behaviour, phase transformations, and mechanical response.

Future LPBF modelling efforts should focus on integrated multiscale frameworks that can simultaneously capture thermal behaviour, melt-pool dynamics, microstructural evolution, and mechanical response. Achieving industrial-scale applicability will require the development of reduced-order models, adaptive meshing techniques, and hybrid modelling strategies to reduce computational cost. There needs to be greater emphasis on developing standardised validation procedures, quantifying uncertainty, and enhancing interoperability among numerical approaches, thereby improving model reliability and transferability [85,94,130–140]. Ultimately, progress is more likely to come from integrating the complementary strengths of existing modelling approaches, rather than from supplanting one approach by another.

8. Emerging LPBF Technologies

8.1. Beam Shaping

Most LPBF systems still use Gaussian beams, mainly because of their ability to concentrate energy, the simplicity of their optical setups, and the large amount of existing process data. But more and more evidence points to a different culprit than energy density: the real problem with Gaussian irradiation is how tightly its thermal energy is concentrated in the melt pool. This concentration results in steep thermal gradients, which increase the risk of keyhole instability, spatter, and epitaxial columnar grain growth that degrades mechanical properties, as well as intensifying recoil pressure, Marangoni convection, and directional heat flow. Tinkering with laser power, scan speed, or hatch spacing only gets you so far in addressing these issues, because the heat source itself does not change. This insight

has prompted research to focus instead on beam shaping, where the aim is not to deliver more energy, but to redistribute the energy delivered to stabilise the melt pool's dynamics and shape its simultaneous solidification. Essentially, beam shaping is a transition from conventional parameter tuning to the direct engineering of the thermal field, providing a new lever for tuning the relationship between the process and the resultant structure in LPBF-processed Inconel superalloys [141,142].

Beam shaping changes the spatial distribution of laser energy but not the total energy input, and can therefore directly impact thermal conditions that determine melt-pool evolution and solidification. Top-hat beam profiles result in a more uniform irradiance than conventional Gaussian beams, helping reduce localised overheating, suppress excessive recoil pressure, and limit steep thermal gradients that drive keyhole instability, spatter formation, and powder denudation. This leads to a more thermally stable melt pool, greater resistance to process parameter variations, and a wider processing window for the manufacturing of high-density Inconel parts. However, this improved uniformity in the energy distribution is achieved at the expense of a lower peak intensity, which can limit melt-pool penetration and affect dimensional accuracy in complex geometries. This trade-off implies that no universal solution exists for the beam profile; rather, the beam geometry should be chosen to balance process stability, geometric fidelity, and microstructural control [51,54,67,101,141,142]. Figure 10 shows that state-of-the-art beam-shaping strategies go beyond traditional top-hat profiles, enabling tools to manipulate the melt-pool heat flow direction and simultaneously control both grain morphology and crystallographic texture. The reduction in grain elongation and the weaker texture intensity observed with engineered beam profiles show that adjusting the laser intensity distribution can directly reshape the thermal field controlling solidification, providing a more effective way of microstructure control than parameter optimisation alone [142].

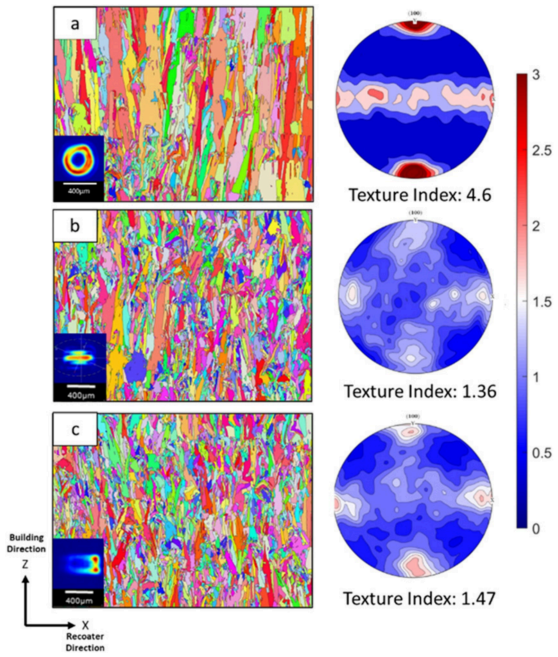


Figure 10. IPF maps and pole figures of diverse samples produced using distinct laser beam profiles: (**a**) ring-shaped, (**b**) Line//SD, and (**c**) chair-shaped [142].

The effect of beam shaping extends beyond the stabilisation of the melt pool—the change of the thermal field directly influences the grain morphology, the crystallographic texture and the resulting mechanical anisotropy. Custom beam profiles lead to a more homogeneous solidification environment, reducing the potential for elongated columnar grains

to grow epitaxially, therefore allowing for more isotropic microstructures and improving the reliability of LPBF manufacturing of Inconel parts. This illustrates the general point that control of heat flow during solidification is as important as control of conventional process parameters to achieve desired structure–property responses [90,119–124]. Promising results have been obtained for melt-pool dynamics and microstructural evolution, but the true industrial potential of beam shaping will be realised through integration with new LPBF technologies rather than as a stand-alone process modification. Future developments should therefore combine beam shaping with multi-laser architectures, advanced in situ monitoring and intelligent process control to establish robust PSPC relationships for industrial-scale manufacturing of Inconel superalloys [94,123,134,136–140].

8.2. Multi-Laser LPBF

Scaling up Inconel component manufacturing has revealed a fundamental weakness of single-laser LPBF: the inherent conflict between throughput and process stability. Increasing the laser power or scanning velocity can increase the deposition rate, but the resulting higher thermal gradients tend to increase residual stress, distortion, and defect formation. This has led to a trend towards multi-laser LPBF (ML-PBF), where multiple lasers are used simultaneously in different scan zones, reducing build times and enabling the fabrication of larger components. Furthermore, ML-PBF not only yields a simple productivity gain but also significantly alters the process's thermal history. Indeed, the concurrent effects of multiple moving heat sources on a single part result in complex thermal fields that cannot be described by single-laser assumptions [143,144].

Despite its productivity advantages, the principal barrier to wider industrial use is frequently reported in the literature to be the thermal interaction between neighbouring laser zones. When multiple melt pools merge in neighbouring scan regions, this alters the local heat build-up, melt-pool flow behaviour, and solidification, leading to inconsistent cooling across stitch boundaries. These overlap zones are more prone to uneven remelting, collisions between molten pools, and droplet ejection, increasing the risk of porosity, surface defects, and localised residual-stress build-up rather than creating a uniform thermal field. Stitch-line defects should therefore be considered not only as geometrical defects but also as sites where differences in local thermal history affect the subsequent microstructural evolution and mechanical behaviour [143,145,146].

Traditional approaches for mitigating these effects have focused on improving laser overlap, scan sequencing, and post-build heat treatment to reduce heterogeneity in stitched regions. Results from Alloy 718 show that stitch zones exhibit microstructural and mechanical differences relative to single-laser regions, but these differences are greatly reduced after hot-isostatic pressing (HIP) and solution-ageing treatment, suggesting that the thermal non-uniformity created during build can be largely eliminated thereafter. However, post-processing alone does not address the root cause of stitch-line formation. Instead, newer multi-laser approaches prefer proactive thermal control using coordinated low-power lasers or supplementary laser sources to distribute heat more evenly, increase melt-pool size, and improve inter-track bonding, while also reducing residual stress and porosity levels. Such findings imply that future ML-PBF research should focus on managing thermal interactions during the build itself, rather than remedying their effects afterwards [143,145].

Multi-laser LPBF is based on coordinated scanning, where multiple lasers simultaneously scan different areas of a large Inconel 718 component, with the stitching zones deliberately moved from layer to layer, as visualised in Figure 11. This method reduces localised heat build-up, spreads the thermal loading across the overlap areas more evenly, and promotes stronger adhesion between layers, thereby reducing the risk of stitch-line defects and high residual stress. The figure also shows that the successful production of large,

high-aspect-ratio parts is not simply a matter of running multiple lasers simultaneously but rather the effective coordination of those lasers to manage the thermal interactions across neighbouring scan fields. Thus, laser coordination and control of stitching zones are important for dimensional accuracy and structural integrity in industrial-scale multi-laser LPBF [143].

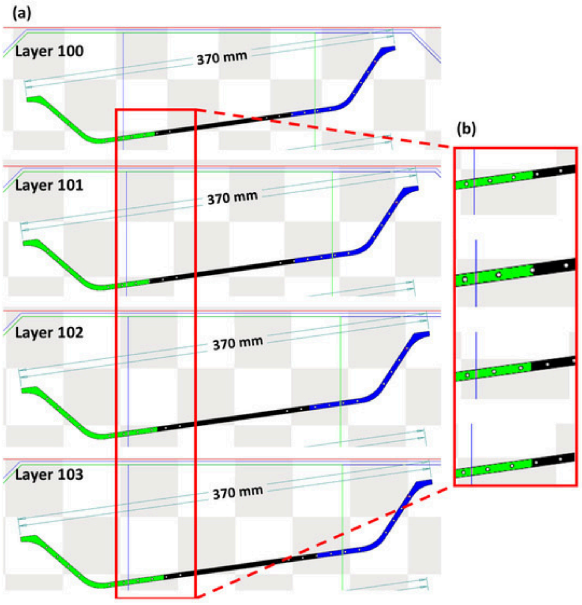


Figure 11. Scanning methodologies employed for ML-PBF in the DMP 500 system. Panel (**a**) illustrates the trajectories of the three lasers, distinguished by green, black, and blue colours, across layers 100 to 103 for the adjusted 1× complete geometry. Panel (**b**) offers a detailed perspective of the left stitching area, emphasising the positional variation of the stitching line across successive layers [143].

The growing implementation of multi-laser LPBF, therefore, marks a transition from merely increasing throughput to controlling complex thermomechanical interactions across large build volumes. Numerical simulations and experimental work indicate that well-designed scan coordination, supplementary laser strategies, and compensation methods can effectively limit distortion and enhance inter-track fusion; however, the ability to predict stitch-zone behaviour under realistic industrial conditions with multiple synchronised lasers and complex part geometries remains limited. Therefore, future research should integrate multi-laser process planning with in situ monitoring, adaptive scan control, and physics-informed predictive models to establish reliable PSPC relationships for the large-scale production of Inconel. This push for a real-time understanding of melt-pool behaviour naturally leads to the next emerging technology, in situ monitoring and synchrotron imaging, where high-speed sensing enables direct observation of the thermal mechanisms responsible for defect formation [143,144,146].

8.3. In Situ Monitoring and Synchrotron Imaging

As LPBF becomes increasingly important for manufacturing critical components in aerospace and energy, the focus on defect detection shifts from traditional post-build inspection to real-time process monitoring. With modern in situ monitoring, you can continuously observe the build so that defects are detected while the part is being built, not after it is complete. Recent advances in optical, thermal, and X-ray sensing are combined to track melt-pool dynamics, thermal changes, and subsurface defect development, laying the groundwork for smarter process qualification and, eventually, closed-loop control [147,148].

The main in situ monitoring techniques used in LPBF are summarised in Figure 12 and grouped into optical, thermal, acoustic, and X-ray-based sensing. Optical monitoring

employs DSLR cameras, photodiodes and digital image correlation (DIC) to observe melt-pool shape, vapour-plume behaviour, and spatter. Thermal monitoring is performed using pyrometers and high-speed cameras to record melt-pool temperatures, cooling rates, and thermal gradients, helping assess process stability. Acoustic sensing detects process-related vibrations and emissions associated with abnormal melting, while X-ray imaging provides direct observation of subsurface melt-pool behaviour, keyhole formation, and pore formation. Collectively, these monitoring methods provide complementary information on the initiation and progression of defects, which can be leveraged to develop reliable real-time monitoring and control strategies for LPBF.

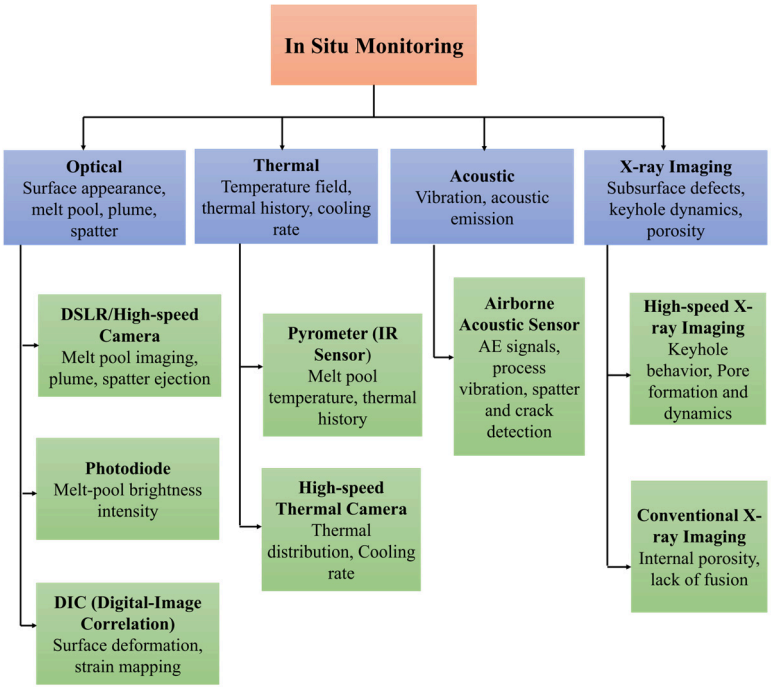


Figure 12. Classification of in situ monitoring techniques utilised in LPBF. Adapted from [147].

The most commonly used monitoring tool is high-speed optical cameras that continuously record melt-pool shape, vapour-plume behaviour, and spatter generation during laser scanning. Early indications of unstable melting, such as deviations in the melt-pool shape and excessive spatter, disrupt powder spreading and increase the risk of lack-of-fusion defects in subsequent layers. Optical monitoring is mainly limited to surface observation, but it is still useful for detecting abnormal melting before the appearance of defects [147–149]. Optical imaging is complemented by thermal monitoring with pyrometers and infrared cameras to measure melt-pool temperature, cooling rate and thermal gradients. Unlike visible-light imaging, thermal measurements follow the evolution of heat distribution during melting and solidification, providing a direct link between thermal instability and defect formation. Combined infrared and synchrotron X-ray imaging has shown that changes in the thermal history correlate closely with melt-pool fluctuations, vapour depression behaviour, and resulting pore formation, indicating that thermal signatures are reliable markers of process stability [150].

The most important advances in process understanding have been achieved through high-speed synchrotron X-ray imaging, which enables direct observation of subsurface melt-pool behaviour that is not possible with conventional optical techniques. This imaging has revealed the dynamic behaviour of keyholes, including pore nucleation, migration, and collapse during laser scanning. These findings indicate that keyhole porosity is caused by unstable vapour depression and melt-pool behaviour, rather than by high laser energy alone.

Synchrotron imaging has also directly verified numerical melt-pool models by visualising the fluid-flow mechanisms that lead to pore entrapment and defect formation [151]. Current research is increasingly focused on integrating multiple sensing modalities rather than a single sensor type. Surface morphology and spatter behaviour are recorded by optical monitoring; pyrometers measure the thermal history; and the evolution of internal defects is monitored by synchrotron X-ray imaging. The integration of these complementary datasets enables more accurate identification of process anomalies and lays the groundwork for machine-learning-based defect prediction and adaptive closed-loop control. Therefore, multi-sensor in situ monitoring is emerging as an enabling technology to improve process repeatability, reduce defect occurrence, and enhance the reliability of LPBF-fabricated Inconel components [147,148,150].

8.4. AI and ML-Driven Optimisation

Artificial intelligence (AI) and machine learning (ML) have become powerful tools for LPBF process optimisation, enabling rapid prediction of process outcomes, defect formation, and parameter selection using experimental, simulation, and in situ monitoring data. Unlike traditional trial-and-error methods, ML algorithms can capture the non-linear relationships between processing parameters, melt-pool behaviour, and manufacturing quality, thereby reducing the experimental effort required for process qualification [152–156]. However, high in-domain prediction accuracy does not necessarily imply physical interpretability or transferability [152,155,156].

A major application area of AI in LPBF is defect prediction based on process parameters, melt-pool characteristics and multi-sensor monitoring data. Artificial neural networks (ANNs), convolutional neural networks (CNNs), support vector machines (SVMs), and ensemble learning algorithms have achieved high accuracy in predicting lack of fusion, keyhole instability, porosity, balling, and cracking across varied processing conditions [152,153,155,156]. The more important distinction is whether these models learn empirical parameter–defect correlations or retain the underlying process physics. Incorporating thermal-history and melt-pool descriptors as intermediate features provides a mechanistic link between processing conditions and defect formation. Hybrid FEM–ANN approaches illustrate this strategy by using simulation-derived melt-pool characteristics to identify defect-prone processing windows in IN718 [153]. Thus, physics–ML integration can improve interpretability by constraining predictions using physically meaningful process states rather than relying solely on raw parameter correlations.

ML is also central in the analysis of the large datasets produced by in situ monitoring systems. The combination of thermal imaging, optical monitoring, photodiode signals, and acoustic emission data, with ML algorithms, allows the detection of process instabilities. Explainable artificial intelligence (XAI) is used to improve model interpretability by identifying the sensor features most strongly associated with defect prediction [152,155,156]. Nevertheless, statistical feature importance is not equivalent to physical causality; an influential sensor feature becomes physically informative only when it can be related to the thermal, melt-pool, or solidification mechanism responsible for the predicted defect [155,156].

Transferability remains a more severe limitation of purely empirical models. A relationship calibrated for one LPBF platform may change with machine configuration, sensing conditions, or processing window, while alloy-dependent thermal and melt-pool responses further complicate transfer across IN625, IN718, and IN738. Consequently, direct transfer of nominal process–defect relationships can produce domain shift. Physics-informed features, physical normalisation, and model recalibration provide a more defensible route towards cross-platform and cross-alloy generalisation [152–156].

Intelligent manufacturing has become a growing focus of research. Multi-sensor monitoring, physics-informed ML, and digital-twin frameworks enable adaptive process control by rapidly assessing process conditions and adjusting parameters. Although fully autonomous closed-loop control is still under development, these integrated approaches hold great promise for enhancing the process stability, repeatability, and manufacturing reliability of LPBF-fabricated Inconel components [152,154,155]. Table 12 summarises representative AI and ML approaches applied to LPBF optimisation, including their learning algorithms, input data, optimisation objectives, advantages, and limitations. These studies collectively suggest a shift from independent defect prediction to integrated intelligent manufacturing systems that combine simulation with in situ sensing and adaptive process control. Collectively, the key challenge is therefore not prediction accuracy alone, but achieving physically interpretable and transferable models.

Table 12. Typical artificial intelligence and machine-learning strategies for optimisation of LPBF processes.

AI/ML Approach	Input Data	Primary Objective	Representative Outputs	Advantages	Limitations	Reference
Artificial Neural Network (ANN)	Laser power, scan speed, layer thickness, melt-pool dimensions, and FEM-derived datasets	Optimising process parameters and forecasting defects	Generation of processing maps, defect-free windows, and predicted melt-pool geometry	Able to model intricate nonlinear behaviour, lowering the need for extensive experimentation	Depends on the availability of large, high-quality training data	[153]
Convolutional Neural Network (CNN)	Melt-pool and thermal imagery, optical monitoring data	Automated classification of defects	Recognition of porosity, lack-of-fusion, delamination, and spatter	Delivers strong classification performance through automated feature extraction	Accuracy is sensitive to image quality and demands significant computing power	[152,156]
Support Vector Machine (SVM)	Acoustic emission, photodiode, and other sensor signals	Classifying process states	Distinguishing stable, conduction, and keyhole-melting regimes	Performs well with smaller datasets and provides reliable classification	Less effective when handling complex, multi-class scenarios	[155,156]
Extreme Gradient Boosting (XGBoost)	Frequency-domain acoustic emission features and statistical parameters	Selecting relevant features and predicting defects	Pinpointing signal features most linked to defect occurrence	Achieves high accuracy while keeping feature importance interpretable	Needs meticulous tuning of hyperparameters	[156]
Explainable Artificial Intelligence (XAI)	Acoustic emission and combined multi-sensor data	Making ML outputs interpretable	Determining which sensor features drive defect formation	Enhances the transparency of models and builds trust for industrial use	Application within LPBF is still in the early stages	[156]
Hybrid Physics–ML (FEM + ANN)	Simulation results validated against experimental data	Speeding up the process of qualification	Processing maps and defect prediction for Inconel 718	Merges physical insight with data-driven refinement	Accuracy is tied to the fidelity of the underlying simulation	[153]
Multi-sensor ML framework	Combined thermal, optical, acoustic, and photodiode signals	Enabling real-time monitoring and optimisation	Ongoing quality evaluation and defect identification	Draws on complementary sensor inputs to boost reliability	Fusing and synchronising diverse sensor data remains difficult	[152,155]
AI-enabled closed-loop control/Digital twin	Live sensor feedback combined with predictive modelling	Achieving adaptive process control	Real-time adjustment of parameters during fabrication	Supports intelligent manufacturing and greater process stability	Industrial adoption is still restricted	[154,155]

Overall, AI/ML can accelerate LPBF optimisation, but empirical models remain constrained by training-domain dependence and limited physical interpretability. Coupling physically meaningful process descriptors with simulation, sensing, and model recalibration provides a more robust route towards transferable defect prediction and adaptive control [152–156]. Long-term reproducibility additionally depends on powder-feedstock evolution, motivating the recyclability considerations discussed next.

8.5. Powder Recyclability and Degradation

Powder recyclability has emerged as a significant consideration in LPBF, given the substantial expense of nickel-based superalloy feedstock and the growing emphasis on sustainable production. In the LPBF process, only a portion of the powder spread onto the bed is consolidated into the finished part, with the unconsolidated material subjected to repeated heating and cooling cycles, spatter generated by the laser, and exposure to the build atmosphere before being reclaimed for further use. While recycling powder offers considerable cost savings, successive reuse gradually alters its properties, thereby affecting process stability, build-to-build consistency, and the overall quality of finished components [157,158].

Degradation in recycled powder stems chiefly from physical and chemical alterations that build up over repeated cycles. Prolonged exposure to high temperatures promotes oxygen absorption and oxide layer formation on particle surfaces, while repeated contact with laser-generated spatter results in partially fused particles, satellite attachment, and irregular particle shapes. At the same time, shifts in particle size distribution, surface texture, and sphericity affect how the powder flows and packs, leading to uneven spreading during the recoating step. These effects, in turn, alter how efficiently the powder absorbs laser energy and how stable the melt pool remains, even under unchanged processing conditions [157–159].

As powder characteristics continue to shift, defect formation during LPBF is directly impacted. Diminished flowability and inconsistent powder deposition increase the likelihood of localised variations in layer thickness, which, in turn, promote lack-of-fusion defects and unstable melting. In addition, elevated oxygen content promotes the formation of oxide inclusions, which serve as preferred sites for crack initiation, while irregular particle shapes and overall powder deterioration contribute to greater porosity and defect concentration. As a result, powder degradation shapes not only the defects that arise during fabrication but also the subsequent microstructural development in the deposited material [159,160].

These microstructural shifts eventually manifest as changes in mechanical properties. Higher levels of oxide inclusions, porosity, and cracking diminish ductility, fatigue life, and overall structural reliability. That said, a number of studies have shown that nickel-based superalloys like Inconel 718 can withstand a moderate number of reuse cycles provided suitable powder management practices are followed, such as sieving, controlled storage conditions, and periodic blending with fresh powder. Thus, the impact of powder recycling is governed not simply by how many times the powder has been reused, but also by how rigorously powder qualification and handling procedures are applied throughout production [157,158].

The main degradation pathways linked to powder recycling and their effects on LPBF performance are outlined in Table 13. This comparison shows that oxygen absorption, changes in particle shape, shifts in particle size distribution, and reduced flowability are closely linked, jointly influencing melt-pool stability, defect generation, and resulting mechanical properties. As such, rigorous powder qualification and reuse practices are critical to sustaining reliable process performance in industrial-scale LPBF manufacturing [157–160].

Table 13. Impact of powder recyclability and degradation on process–structure–property evolution during LPBF of nickel-based superalloys.

Powder-Degradation Mechanism	Cause During Powder Reuse	Change in Powder Characteristics	Effect on LPBF Process	Resulting Defects/Microstructure	Impact on Mechanical Properties	References
Oxygen pickup and oxidation	Cyclical heat exposure, contact with ambient atmosphere, and handling during processing	Elevated oxygen levels, formation of oxide films and inclusions	Disrupts melt-pool chemistry and promotes instability	Oxide inclusions, sites favouring crack initiation, and non-uniform microstructure	Diminished ductility, fatigue life and fracture toughness	[158,159]
Particle morphology evolution	Adhesion of laser spatter, presence of partially melted particles, and cumulative recycling	Formation of satellite particles, irregular shapes, and lower sphericity	Impaired powder spreading and inconsistent layer formation	Greater incidence of lack-of-fusion and pore development	Reduced density and weaker tensile behaviour	[157–159]
Particle size distribution (PSD) evolution	Sieving effects, incorporation of spatter, and preferential depletion of fine particles	Shift toward a coarser or wider particle size range	Lower packing efficiency and irregular powder bed	Instability in the melt pool and elevated porosity	Diminished process repeatability and dimensional precision	[157,158]
Flowability degradation	Increased surface roughness, oxidation, and morphological changes	Reduced flow and spreading behaviour	Inconsistent powder layering and variable thickness	Lack-of-fusion defects and incomplete fusion	Lower strength, ductility, and reproducibility	[157,158]
Absorptivity variation	Surface oxide formation and altered particle surface condition	Change in how laser energy is absorbed	Fluctuations in melt-pool temperature and shape	Keyhole-related instability or insufficient melting	Variable mechanical performance	[157]
Powder contamination	Vapour condensation and exposure to the surrounding environment	Altered chemical makeup and inclusion generation	Irregular melting response	Higher inclusion levels and greater defect concentration	Shortened fatigue life and compromised structural reliability	[157,159]
Repeated powder recycling	Successive reuse cycles lacking proper qualification	Combined physical and chemical deterioration	Greater variability throughout the process	Accumulating defects and an inconsistent microstructure over time	Decline in properties once reuse surpasses acceptable thresholds	[157–160]
Powder qualification and management	Sieving practices, inert-atmosphere storage, and blending in virgin powder	Preserves consistent powder quality	Stable melt-pool behaviour and even powder spreading	Fewer defects and a more uniform microstructure	Better repeatability and enhanced mechanical properties	[157,158,160]

Within the PSPC framework, powder properties should therefore be treated as dynamic material-state variables rather than fixed process inputs. Each build/recovery cycle can alter oxygen content, particle-size distribution, morphology, flowability, and absorptivity, and these properties should accordingly be reassessed before the powder is reused [157–160]. This establishes an inter-build feedback pathway running from powder recovery/reuse to degradation, quality assessment, and the decision to reuse, refresh, or reject the powder, ultimately updating the feedstock state for the next build. The Control component of PSPC thus extends beyond intra-build adjustment of processing conditions to encompass build-to-build feedstock management, directly linking powder qualification to subsequent melt-pool stability, defect evolution, and part quality.

In summary, powder recyclability is more than a cost-saving measure; it has become a decisive factor in achieving reliable LPBF manufacturing results. The progressive evolution of oxygen content, particle shape, flow behaviour, and absorptivity directly impacts melt-

pool dynamics, defect generation, and the mechanical properties ultimately obtained, highlighting the need for systematic protocols governing powder qualification and reuse. Therefore, from the PSPC perspective, Powder recycling links the material state and Control parts through ongoing feedstock qualification, in which the new powder condition becomes the material input for the next build cycle. Hence, sound powder management is an important control lever to sustain a stable process–structure–property relationship and to achieve consistent and reliable production of high-performance Inconel components by LPBF.

9. Digital Twin and AI Framework for Predictive LPBF

Driven by the limitations of physics-based simulations and data-driven optimisation alone, digital twin (DT) frameworks have emerged for LPBF. FEM accurately predicts thermal history, melt-pool behaviour, and residual stress. However, its computational demands limit its suitability for real-time applications. In contrast, machine learning (ML) accelerates prediction but heavily relies on the quality and extent of the training data and often lacks physical interpretability. These limitations are addressed by digital twins that couple physics-based modelling, in situ monitoring, and AI within a common cyber-physical framework to enable real-time prediction, process monitoring, and adaptive control [138,139,152,153,161]. To avoid this integration becoming a computationally efficient black-box surrogate, physics-based, and data-driven components should be connected through physically meaningful thermal and melt-pool states rather than solely nominal process parameters [152,153].

Figure 13 shows the overall architecture of a digital-twin framework for LPBF. The physical manufacturing system is connected to its virtual twin through a constant two-way data flow. Sensor data are used in real time to predict process behaviour and component quality using physics-based and data-driven models. The resulting outputs are stored, visualised, and analysed, providing the basis for continuous process monitoring and well-informed decision-making. Finally, a closed-loop feedback mechanism completes the framework, enabling adaptive tuning of process parameters and thereby improving the reliability, quality, and productivity of the manufacturing process [134].

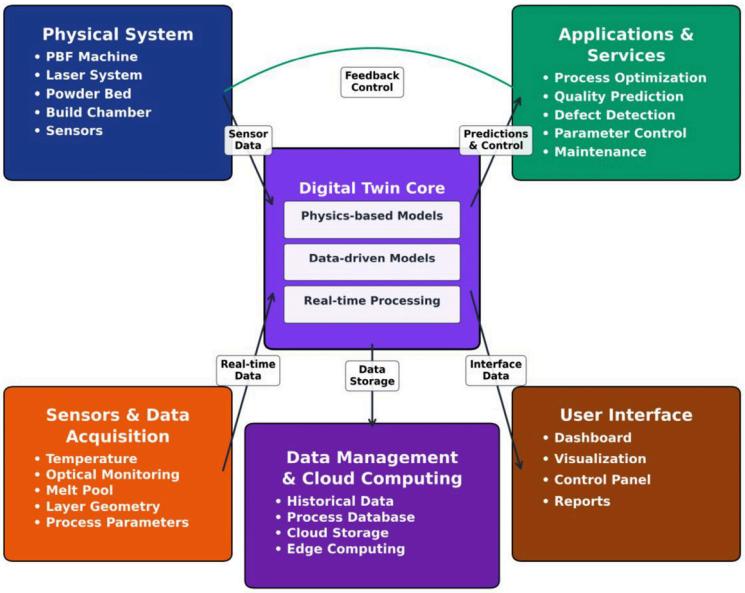


Figure 13. Digital-twin framework for the additive manufacturing process [134].

Hybrid modelling marries the computational speed of AI-based methods with the physical accuracy of numerical simulations. For example, melt-pool features extracted through FEM have been used to train artificial neural networks that can quickly identify processing windows associated with lack-of-fusion, balling, and keyhole defects in LPBF-fabricated Inconel 718, significantly reducing computational cost without compromising predictive accuracy [152]. Here, the value of hybridisation extends beyond computational acceleration: simulation-derived melt-pool features provide an intermediate physical link between process inputs and ML-predicted defects [152,153]. This hybrid approach further enhances the predictive capabilities of digital twins by fusing data from multiple sensors, including thermal imaging, optical monitoring, photodiode signals and acoustic emission. Digital twins enable early detection of process instabilities by combining these data streams with ML algorithms, reducing reliance on post-process inspection and destructive testing [153,154,161].

Digital twins do more than observe the process; they also allow the transition from predictive manufacturing to adaptive process control. The digital twin enables dynamic tuning of process parameters, such as laser power, scan speed, and hatch spacing, by continuously comparing predicted and measured process states, thereby compensating for variations in melt-pool behaviour and thermal history. While fully autonomous closed-loop control is still an active area of development, recent research indicates that an interesting path towards intelligent LPBF systems is the combination of digital twins and AI-assisted decision-making, leading to improved process repeatability, reduced defect formation, and increased manufacturing reliability [138,139,161]. Digital twins provide an integrated platform for linking processing conditions, thermal behaviour, microstructural evolution, defect formation, and component performance through continuous feedback and adaptive control. This capability provides the technological basis of the integrated PSPC framework proposed in this review.

In this architecture, beam shaping, multi-laser processing, in situ monitoring, powder-state management, and digital twins are complementary elements of a single closed-loop control system. The actuation layer is controlled by beam shaping and multi-laser systems to manage the spatial energy input and melt-pool behaviour. In situ monitoring provides real-time thermal and melt-pool state information. Physics-based and AI models in the digital twin assimilate these measurements to estimate the process state, predict instability, and decide on corrective actions. The adjustment of laser power, scan speed, beam profile, or laser allocation feeds the resulting decisions back to the actuation layer, forming a sensing–prediction–decision–actuation loop. Powder recycling, including powder-quality assessment to update the state of the feedstock and model inputs prior to further processing, further improves this control [136–139,152–154,157–161]. The integrated technical route thus connects actuation, LPBF process response, sensing, state prediction, decision-making, and corrective actuation in a closed-loop sequence, whereas a parallel pathway, including powder assessment, feedstock-state updating and subsequent build-cycle adjustment, supports build-to-build control. Together, both pathways enable real-time and inter-build optimisation within the PSPC framework.

Despite this potential, several barriers restrict the industrial implementation of LPBF digital twins. The lack of standardised, interoperable datasets and variations in machine architecture, sensing systems, and processing conditions limit model robustness and transferability. This limitation becomes more critical across different LPBF platforms and Inconel compositions because equivalent nominal-process parameters do not necessarily represent equivalent physical-process states. Direct transfer of empirical relationships can therefore introduce a domain shift, requiring physical normalisation and model recalibration for cross-platform and cross-alloy deployment. Other challenges include the computational

expense of coupling real-time monitoring with high-fidelity multiphysics simulations, heterogeneous sensor-data fusion, limited cross-platform validation, software interoperability, data security, and infrastructure requirements. Future work should therefore prioritise standardised data frameworks, computationally efficient and physically interpretable hybrid models, robust multi-sensor fusion, and rigorous cross-platform and cross-alloy validation to enable scalable and reliable digital twins for predictive modelling of LPBF-processed Inconel alloys [136–139].

10. Scientific Synthesis and Future Research Roadmap

10.1. Scientific Synthesis of the PSPC Framework

The literature reviewed in this work shows that isolated process variables or individual material responses cannot simply explain the performance of LPBF-fabricated Inconel alloys. Instead, component quality results from a hierarchical, tightly coupled PSPC relationship, in which each stage controls the subsequent evolution of the material and interacts with previous stages via feedback mechanisms. In this framework, powder characteristics and processing parameters determine the initial thermal conditions governing melt-pool formation, whereas melt-pool dynamics determine the local temperature distribution, fluid flow behaviour, and solidification conditions. These thermal phenomena, in turn, control grain morphology, crystallographic texture, and phase evolution, which collectively control defect formation, residual-stress development, and ultimately the mechanical performance of LPBF-fabricated components. These stages are not independent scientific phenomena but a connected sequence of local changes at one level that ripple through the whole manufacturing process.

The review also indicates that melt-pool dynamics is the fundamental physical relationship between processing conditions and microstructural evolution. Thermal gradients, cooling rates, and melt-pool stability are affected by changes in laser power, scan speed, hatch spacing, layer thickness, and powder characteristics, thereby controlling solidification behaviour and competitive grain growth. The resulting grain morphology directly influences the formation of porosity, lack of fusion defects, keyhole instability, cracking, and residual stresses, which, in turn, dictate tensile strength, ductility, fatigue resistance, and high-temperature performance. Therefore, process optimisation should be viewed not as the adjustment of individual processing parameters but as the systematic control of melt-pool behaviour that governs the whole process–structure–property relationship.

Another important result of this review concerns the evolution of predictive manufacturing strategies. While traditional experimental optimisation and standalone numerical simulations have made significant contributions to understanding LPBF, they are insufficient for reliable real-time process optimisation when used independently. Recent progress indicates that combining multiphysics simulations, in situ monitoring, and artificial intelligence enables continuous prediction of process behaviour, while digital-twin technologies provide the framework to translate these predictions into adaptive process control. Thus, the Control component of the PSPC framework extends traditional parameter optimisation by providing continuous feedback between the physical manufacturing process and its virtual counterpart, creating a closed-loop manufacturing paradigm that can improve process repeatability and defect formation. The unified PSPC framework proposed in this review, therefore, provides a scientific perspective beyond the individual topics discussed in the previous sections. Instead of treating melt-pool physics, grain evolution, defect formation, residual stress, mechanical behaviour, computational modelling, and intelligent manufacturing as separate research areas, the framework describes their intrinsic interdependencies within a single predictive manufacturing philosophy. This integrated understanding provides the scientific foundation for the future development of physics-informed, data-driven

and closed-loop LPBF systems capable of producing high-performance Inconel components with enhanced reliability, consistency and manufacturing efficiency [137–139]. The proposed PSPC framework, summarised in Figure 14, combines the main scientific mechanisms of LPBF of Inconel alloys into a holistic workflow. The framework shows how melt-pool dynamics, resulting from processing parameters and the material state, in turn control solidification behaviour, grain evolution, defect formation, and the resulting mechanical properties. It further underlines the sequential and interdependent character of these process–structure–property relationships. The framework proposes a closed-loop approach to intelligent, predictive LPBF manufacturing using digital twin technologies, including AI, in situ monitoring, predictive modelling, and feedback control.

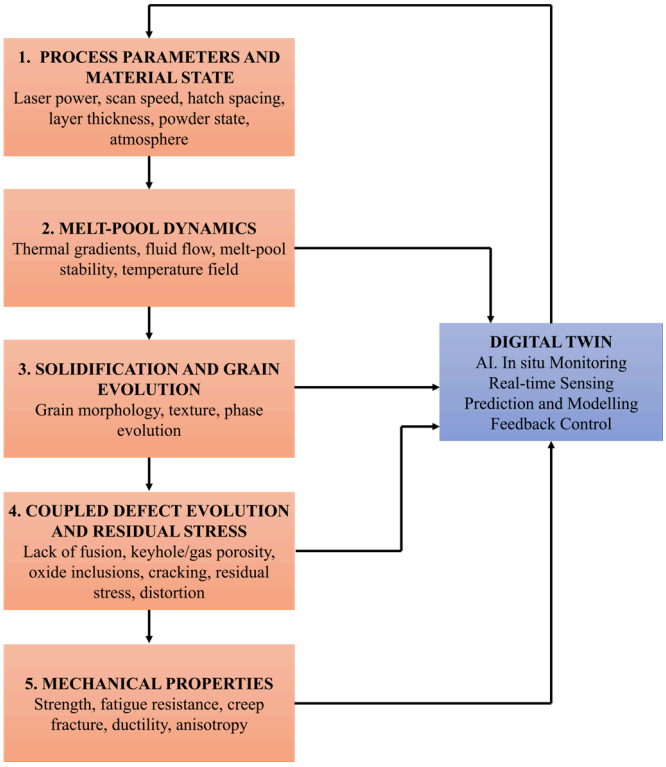


Figure 14. Scientific synthesis of the process–structure–property–control (PSPC) framework showing the interrelated relationships between process parameters, melt-pool dynamics, microstructural evolution, defect formation, mechanical performance, and digital-twin-enabled feedback control for predictive LPBF of Inconel alloys.

The applicability of the proposed PSPC framework should nonetheless be considered within the compositional and metallurgical boundaries of the alloy system in question. The framework as presented is derived primarily from IN625, IN718, and IN738/IN738LC, alloys that exhibit distinct strengthening mechanisms and solidification behaviour within the Inconel family. At a fundamental level, the relationships connecting processing conditions, heat transfer and melt-pool dynamics, solidification behaviour, grain evolution, defect formation, and resulting properties can be extended to other Ni-based superalloys, given that comparable process–structure–defect–property relationships have been extensively documented across additively manufactured Ni-based systems [162]. This transferability, however, does not mean that alloy-specific quantitative criteria can be applied without modification. Thermophysical properties, solidification range, solute partitioning, microsegregation, precipitation kinetics, and cracking susceptibility all require recalibration based on alloy chemistry. This distinction becomes especially critical for high-Al/Ti γ'-strengthened superalloys, where γ' precipitation together with segregation-assisted solidification, liqua-

tion, and strain-age cracking can emerge as the dominant metallurgical responses [163,164]. Similarly, Nb- and Mo-rich segregation can drive interdendritic Laves-phase formation in susceptible compositions, necessitating explicit consideration of phase stability and local chemistry [164]. Consequently, extending the PSPC framework beyond IN625, IN718, and IN738/IN738LC should preserve its core physical architecture while incorporating alloy-specific thermodynamic, kinetic, and constitutive descriptions, rather than transferring process-window boundaries in a direct, unmodified manner.

10.2. Core Scientific Insights

Scientific Insight 1. Melt-pool dynamics dominate the physical link between processing conditions and component performance.

Laser power, scan speed, hatch spacing, and layer thickness are typically considered the main process parameters in LPBF, but their effects on component quality are essentially indirect. These parameters primarily determine the distribution of thermal energy in the powder bed, which, in turn, influences melt-pool geometry, fluid-flow behaviour, and solidification conditions. Therefore, melt-pool stability controls the transition between conduction-mode melting, lack-of-fusion, and keyhole regimes, and hence grain morphology, defect formation, and residual-stress evolution. This suggests that future optimisation efforts should focus on controlling melt-pool behaviour rather than fine-tuning individual processing parameters, adopting a more physically based approach to achieve consistent manufacturing results.

Scientific Insight 2. Microstructure is the missing link between the thermal history and engineering performance.

The literature consistently demonstrates that the thermal gradients and cooling rates imposed during LPBF do not directly determine mechanical properties but instead govern grain morphology, crystallographic texture, and phase evolution. These microstructural features then determine the strength, ductility, fatigue resistance, creep behaviour, and fracture response. Hence, the microstructure is the key mediator between processing conditions and the engineering performance. This means that reliable property optimisation requires simultaneous control over the thermal history and solidification behaviour and is not just about post-process mechanical testing.

Scientific Insight 3. Defects are not manufacturing defects but process instabilities.

Porosity, lack of fusion defects, keyhole collapse, hot cracking, and residual stresses are often investigated as individual failure modes. The evidence accumulated throughout this article, however, points to a common origin of these defects: melt-pool dynamics and thermal evolution instability. The initiation and growth of defects are governed by changes in energy input, powder properties, and local heat accumulation, whereas subsequent microstructural modifications govern the impact on structural integrity. Defect mitigation efforts should then focus on stabilising the underlying thermal and fluid-flow phenomena rather than on individual defect types separately.

Scientific Insight 4: Predictive LPBF is achieved through the integration of physics-based modelling and artificial intelligence.

No single approach, experimental optimisation, numerical simulation, or machine learning can fully capture the complexity of LPBF processing by itself. Physics-based models provide mechanistic insight and predictive strength while AI facilitates rapid interpretation of high-dimensional process data and real-time decision-making. The future of predictive LPBF, therefore, lies in hybrid frameworks that combine multiphysics simulations, in situ monitoring, and data-driven learning in unified predictive systems.

This integration enables continuous improvement of process predictions while preserving physical consistency, thereby bridging the gap between computational precision and industrial relevance.

Scientific Insight 5: Physics-informed feedback transforms LPBF from an open-loop PSP relationship into a closed-loop Process–Structure–Property–Control system.

Among the most significant developments identified in this review is the shift from the conventional forward process–structure–property relationship toward a closed-loop framework, in which predicted or monitored physical process states inform upstream process control. Within the proposed PSPC framework, the Control element is therefore not merely the addition of digital twin, AI, or in situ monitoring technologies. Rather, it represents a mechanism-informed feedback pathway that connects measurable or predicted intermediate physical states, particularly melt-pool stability, thermal history, and solidification behaviour, back to controllable front-end processing parameters. Deviations in these intermediate states can signal changes in energy transfer, melt-pool stability, or solidification conditions before such changes manifest as undesirable microstructural features or defects, thereby allowing corrective adjustment of processing conditions at an earlier point in the causal chain. Digital twins supply the enabling infrastructure for this feedback by integrating sensor data, computational models, and intelligent algorithms to track process evolution and support adaptive process optimisation. Monitoring, AI, and digital twins therefore function as enabling technologies, while the physical basis of the Control component lies in using process-state information to regulate the upstream mechanisms that govern the evolution of structure and properties. This shift establishes a closed-loop manufacturing paradigm in which processing conditions are continuously refined based on the evolving physical state of the process, rather than solely on final component quality. Accordingly, the next generation of LPBF systems is expected to progress from parameter-driven manufacturing toward intelligent, self-monitoring, and self-optimising production platforms capable of reliably and repeatedly producing high-performance Inconel components.

10.3. Future Research Roadmap

The scientific synthesis presented in this review highlights that the further development of LPBF for Inconel alloys will need to move from incremental tuning of individual process parameters to the development of integrated, predictive, and autonomous manufacturing systems. Such a transition requires concerted progress in modelling, process monitoring, intelligent control, and experimental validation. Given the current state of the field, the following research directions are likely to have the greatest scientific and industrial value.

Developing fully coupled multi-scale modelling frameworks. Future work should aim to develop computational frameworks that directly link thermo-fluid dynamics, solidification, grain evolution, phase transformations, and thermomechanical behaviour within a single simulation environment. This integration would increase the predictive power of the LPBF models and strengthen the process–structure–property relationships needed for component-scale optimisation.

Physics-informed AI for Predictive Manufacturing. Future AI models should include physical constraints derived from heat transfer, fluid flow, and solidification principles, rather than relying solely on data-driven learning. Physics-informed AI has the potential to improve model generalisation, reduce the need for training data, and increase confidence in predictions across various manufacturing conditions.

Closed-loop process control with a digital twin. The next step in the evolution of digital twins is to go beyond monitoring processes and enable autonomous decision-making by integrating real-time sensing, predictive simulations, and adaptive control

algorithms. Such systems would enable continuous adjustment of process parameters during fabrication, improving repeatability, reducing defect rates, and accelerating the industrial qualification of LPBF components.

Standardised datasets and validation protocols. The lack of common benchmark datasets and standard validation procedures remains a major hurdle to comparing computational models, AI algorithms, and experimental studies. Standardised data formats and validation methods, along with open benchmark problems, would improve model reproducibility and enable wider industrial adoption of predictive manufacturing methods.

Integrated quality of powder, process, and part performance. Future qualification approaches should instead be integrated to account for powder characteristics, process stability, microstructural evolution, and mechanical performance as a single system, rather than separate stages. Such holistic qualification frameworks would improve consistency in manufacturing, enable certification of safety-critical components, and increase confidence in LPBF-fabricated Inconel alloys for aerospace, energy, and high-temperature engineering applications.

Collectively, these research directions chart a pathway toward next-generation LPBF systems that incorporate multiscale modelling, intelligent monitoring, physics-informed AI, and digital-twin technologies into a unified process–structure–property–control framework. Moving from a descriptive understanding of the process to predictive and adaptive manufacturing will be critical to enable reliable, efficient, and industrially scalable production of high-performance Inconel components. In this sense, the PSPC framework proposed in this review is not only a scientific interpretation of the current state of LPBF research but also a strategic roadmap for future progress in intelligent metal additive manufacturing.

11. Conclusions

LPBF has emerged as a critical manufacturing route for producing high-performance Inconel components with complex geometry for aerospace, energy, and industrial applications. This review has shown that component quality and reproducibility are governed by a chain of tightly coupled thermal, metallurgical, and mechanical phenomena rather than by any single process parameter. It has proposed the PSPC framework as a unified basis for linking processing conditions to microstructure, defects, and performance. The principal conclusions are summarised below.

Melt-pool physics governs LPBF of Inconel alloys. Laser–powder interaction determines melt-pool stability, thermal gradients, fluid flow, and solidification pathways, which in turn control grain morphology, crystallographic texture, residual-stress development, and defect formation. Process optimisation is therefore best directed at controlling melt-pool behaviour rather than tuning individual parameters in isolation.

Modelling and in situ monitoring approaches provide complementary, not complete, insight into LPBF. Thermal, thermo-mechanical, CFD, phase-field, cellular automata, and crystal-plasticity models have advanced understanding of temperature evolution, melt-pool behaviour, grain growth, and mechanical response, while in situ sensing captures transient process behaviour experimentally. A computationally efficient multiscale framework linking melt-pool physics to part-scale performance remains a major open challenge.

Traditional parameter-based optimisation (laser power, scan speed, hatch spacing, layer thickness) has improved density and mechanical performance but treats processing, microstructural evolution, and component performance as separate stages. Emerging technologies including beam shaping, multi-laser processing, adaptive scan strategies, machine learning, and digital twins are converging into integrated systems of real-time sensing, physics-based modelling, and data-driven decision-making, addressing

this limitation through closed-loop control, improved process stability, and component-specific optimisation.

Realising predictive, adaptive LPBF manufacturing requires robust multiscale frameworks integrating melt-pool dynamics, solidification behaviour, grain evolution, residual stress, and mechanical performance, together with standardised datasets, benchmarking methods, and validation protocols across LPBF platforms and alloy systems.

Future LPBF systems should shift from parameter-driven manufacturing toward a knowledge-driven, microstructure-by-design paradigm, integrating physics-based modelling, real-time sensing, artificial intelligence, and digital twins within a unified PSPC framework to enable reproducible, defect-controlled, application-specific Inconel components for aerospace, energy, defence, and biomedical applications.

Taken together, these findings indicate that the future of LPBF for Inconel alloys depends not only on process parameter optimisation, but also on the capability to intelligently sense, predict, and control microstructural evolution in real time. Advancing the PSPC framework through integrated modelling, monitoring, and control offers a pathway toward autonomous, defect-controlled additive manufacturing of Inconel components for next-generation engineering applications.

Funding: This research received no external funding.

Data Availability Statement: No new data were created or analyzed in this study. Data availability does not apply to this review article.

Conflicts of Interest: The authors declare no conflict of interest.

Abbreviations

The following abbreviations are used in this manuscript:

LPBF	Laser powder bed fusion
PSPC	Process–structure–property–control
CALPHAD	Calculation of phase diagrams
VED	Volumetric energy density
IN738LC	Inconel 738 low carbon
CET	Columnar to equiaxed transition
KAM	Kernal average misorientation
GND	Geometrically necessary dislocation
Ni	Nickel
Nb	Niobium
Mo	Molybdenum
HIP	Hot isostatic pressing
FEM	Finite-element method
DIC	Digital image correlation
DSLR	Digital single-lens reflex
AI	Artificial intelligence
ML	Machine learning
ANNs	Artificial neural networks
CNNs	Convolutional neural networks
SVMs	Support vector machines
XAI	Explainable artificial intelligence
DT	Digital twin

References

1. Volpato, G.M.; Tetzlaff, U.; Fredel, M.C. A comprehensive literature review on laser powder bed fusion of Inconel superalloys. *Addit. Manuf.* **2022**, *55*, 102871. [CrossRef]
2. Karia, M.C.; Popat, M.A.; Sangani, K.B. Selective laser melting of Inconel super alloy-a review. In *AIP Conference Proceedings*; AIP Publishing: Melville, NY, USA, 2017; Volume 1859. [CrossRef]
3. Detrois, M.; Rozman, K.A.; Jablonski, P.D.; Hawk, J.A. Compositional Design and Mechanical Properties of INCONEL® Alloy 725 Variants. In *Proceedings of the 9th International Symposium on Superalloy 718 & Derivatives: Energy, Aerospace, and Industrial Applications*; Ott, E., Liu, X., Andersson, J., Bi, Z., Bockenstedt, K., Dempster, I., Groh, J., Heck, K., Jablonski, P., Kaplan, M., et al., Eds.; The Minerals, Metals & Materials Series; Springer: Cham, Switzerland, 2018. [CrossRef]
4. Sezek, S.; Ispirlioğlu Kara, G.; Bayram, S.; Aksakal, B. Wear Behavior Of Inconel 925 Alloy After Plastic Deformation. *Int. J. Mod. Manuf. Technol.* **2023**, *XV*, 167–172. [CrossRef]
5. Ananthapadmanaban, D.; Praveen, J.; Vijayaram, T.R.; Natarajan, M.P.; Ramarao, M. Mechanical Properties of INCONEL 625 Alloy in Cast and Extruded Conditions. *Int. J. Veh. Struct. Syst.* **2022**, *14*, 424–428. [CrossRef]
6. Son, K.T.; Phan, T.Q.; Levine, L.E.; Kim, K.S.; Lee, K.A.; Ahlfors, M.; Kassner, M.E. The creep and fracture properties of additively manufactured inconel 625. *Materialia* **2021**, *15*, 101021. [CrossRef]
7. Zhang, M.; Zhu, Z.; Zhang, L.; Gao, M.; Gao, J.; Du, M.; Wang, B. Understanding microstructure evolution and corrosion behavior of wire arc cladding inconel 625 Superalloy by Thermodynamic approaches. *J. Alloys Compd.* **2023**, *947*, 169530. [CrossRef]
8. Chattopadhyay, P.; Bhattacharjee, B.; Kumar, R.; Panda, A.; Sahoo, A.K.; Das, D. Research progress on laser beam machining on inconel 718 alloys: A review. In *AIP Conference Proceedings*; AIP Publishing: Melville, NY, USA, 2024; Volume 3007. [CrossRef]
9. Xu, J.; Ding, Y.; Gao, Y.; Liu, B.; Xue, S.; Hu, Y.; Zhang, D.; Song, X. Improving high-temperature mechanical properties of laser powder bed-fused Inconel 738 alloy by hot isostatic pressing: Tailoring precipitates and healing defects. *Mater. Sci. Eng. A* **2023**, *862*, 144285. [CrossRef]
10. Kurdi, A.; Aldoshan, A.; Alshabouna, F.; Alodadi, A.; Degnah, A.; Alnaser, H.; Tabbakh, T.; Basak, A.K. Investigation into the Microstructure and Hardness of Additively Manufactured (3D-Printed) Inconel 718 Alloy. *Materials* **2023**, *16*, 2383. [CrossRef] [PubMed]
11. Ajay, V.; Babu, N.K.; Ashfaq, M.; Kumar, T.M.; Krishna, K.V. A Review on Rotary and Linear Friction Welding of Inconel Alloys. *Trans. Indian Inst. Met.* **2021**, *74*, 2583–2598. [CrossRef]
12. Soffel, F.; Eisenbarth, D.; Hosseini, E.; Wegener, K. Interface strength and mechanical properties of Inconel 718 processed sequentially by casting, milling, and direct metal deposition. *J. Mater. Process. Technol.* **2021**, *291*, 117021. [CrossRef]
13. Balbaa, M.; Mekhiel, S.; Elbestawi, M.; McIsaac, J. On selective laser melting of Inconel 718: Densification, surface roughness, and residual stresses. *Mater. Des.* **2020**, *193*, 108818. [CrossRef]
14. Kladovasilakis, N.; Charalampous, P.; Tsongas, K.; Kostavelis, I.; Tzovaras, D.; Tzetzis, D. Influence of Selective Laser Melting Additive Manufacturing. Parameters in Inconel 718 Superalloy. *Materials* **2022**, *15*, 1362. [CrossRef] [PubMed]
15. Murr, L.E.; Gaytan, S.M.; Ramirez, D.A.; Martinez, E.; Hernandez, J.; Amato, K.N.; Shindo, P.W.; Medina, F.R.; Wicker, R.B. Metal fabrication by additive manufacturing using laser and electron beam melting technologies. *J. Mater. Sci. Technol.* **2012**, *28*, 1–14. [CrossRef]
16. Gu, D.; Shi, X.; Poprawe, R.; Bourell, D.L.; Setchi, R.; Zhu, J. Material-structure-performance integrated laser-metal additive manufacturing. *Science* **2021**, *372*, eabg1487. [CrossRef] [PubMed]
17. Lykov, P.A.; Baitimerov, R.M.; Vaulin, S.D. Influence of SLM Process Parameters on Porosity of Nickel Base Heat Resistance Alloy EP648. In *Materials Science Forum*; Trans Tech Publications, Ltd.: Freienbach, Switzerland, 2016; Volume 843, pp. 253–258. [CrossRef]
18. Bean, G.E.; Witkin, D.B.; McLouth, T.D.; Zaldivar, R.J. The effect of laser focus and process parameters on microstructure and mechanical properties of SLM Inconel 718. In *Laser 3D Manufacturing*; SPIE: Bellingham, WA, USA, 2018; Volume 10523. [CrossRef]
19. Ortiz Rios, C.; Amine, T.; Newkirk, J.W. Tensile behavior in selective laser melting. *Int. J. Adv. Manuf. Technol.* **2018**, *96*, 1187–1194. [CrossRef]
20. Shifeng, W.; Shuai, L.; Qingsong, W.; Yan, C.; Sheng, Z.; Yusheng, S. Effect of molten pool boundaries on the mechanical properties of selective laser melting parts. *J. Mater. Process. Technol.* **2014**, *214*, 2660–2667. [CrossRef]
21. Zerbst, U.; Hilgenberg, K. Damage development and damage tolerance of structures manufactured by selective laser melting–a review. *Procedia Struct. Integr.* **2017**, *7*, 141–148. [CrossRef]
22. Scime, L.; Beuth, J. Melt pool geometry and morphology variability for the Inconel 718 alloy in a laser powder bed fusion additive manufacturing process. *Addit. Manuf.* **2019**, *29*, 100830. [CrossRef]
23. Baldi, N.; Giorgetti, A.; Palladino, M.; Giovannetti, I.; Arcidiacono, G.; Citti, P. Study on the Effect of Preheating Temperatures on Melt Pool Stability in Inconel 718 Components Processed by Laser Powder Bed Fusion. *Metals* **2023**, *13*, 1792. [CrossRef]
24. Mercelis, P.; Kruth, J.P. Residual stresses in selective laser sintering and selective laser melting. *Rapid Prototyp. J.* **2006**, *12*, 254–265. [CrossRef]

25. Zaeh, M.F.; Branner, G. Investigations on residual stresses and deformations in selective laser melting. *Prod. Eng. Res. Dev.* **2010**, *4*, 35–45. [CrossRef]
26. He, X.; Yang, B.; Kong, D.; Dai, K.; Ni, X.; Chen, Z.; Dong, C. An integrated multiscale simulation guiding the processing optimisation for additively manufactured nickel-based superalloys. *Virtual Phys. Prototyp.* **2024**, *19*, e2313661. [CrossRef]
27. Sarkar, D.; Angshuman, K.; Abhay, S. Advances in computational modeling for laser powder bed fusion additive manufacturing: A comprehensive review of finite element techniques and strategies. *Addit. Manuf.* **2024**, *85*, 104157. [CrossRef]
28. Zhou, W.; Tian, Y.; Tan, Q.; Qiao, S.; Luo, H.; Zhu, G.; Shu, D.; Sun, B. Effect of carbon content on the microstructure, tensile properties and cracking susceptibility of IN738 superalloy processed by laser powder bed fusion. *Addit. Manuf.* **2022**, *58*, 103016. [CrossRef]
29. Samuel, C.; Arivarasu, M.; Prabhu, T.R. High temperature dry sliding wear behaviour of laser powder bed fused Inconel 718. *Addit. Manuf.* **2020**, *34*, 101279. [CrossRef]
30. Nguyen, Q.B.; Nai, M.L.S.; Zhu, Z.; Sun, C.N.; Wei, J.; Zhou, W. Characteristics of Inconel powders for powder-bed additive manufacturing. *Engineering* **2017**, *3*, 695–700. [CrossRef]
31. Ravichander, B.B.; Rahimzadeh, A.; Farhang, B.; Shayesteh Moghaddam, N.; Amerinatanzi, A.; Mehrpouya, M. A Prediction Model for Additive Manufacturing of Inconel 718 Superalloy. *Appl. Sci.* **2021**, *11*, 8010. [CrossRef]
32. Kumar, P.; Farah, J.; Akram, J.; Teng, C.; Ginn, J.; Misra, M. Influence of laser processing parameters on porosity in Inconel 718 during Additive Manufacturing. *Int. J. Adv. Manuf. Technol.* **2019**, *103*, 1497–1507. [CrossRef]
33. Gradl, P.R.; Tinker, D.C.; Ivester, J.; Skinner, S.W.; Teasley, T.; Bili, J.L. Geometric feature reproducibility for laser powder bed fusion (L-PBF) Additive Manufacturing with Inconel 718. *Addit. Manuf.* **2021**, *47*, 102305. [CrossRef]
34. Gamon, A.; Arrieta, E.; Gradl, P.R.; Katsarelis, C.; Murr, L.E.; Wicker, R.B.; Medina, F. Microstructure and hardness comparison of as-built Inconel 625 alloy following various additive manufacturing processes. *Results Mater.* **2021**, *12*, 100239. [CrossRef]
35. Nayak, S.K.; Mishra, S.K.; Jinoop, A.N.; Paul, C.P.; Bindra, K.S. Experimental Studies on Laser Additive Manufacturing of Inconel-625 Structures Using Powder Bed Fusion at 100 μm Layer Thickness. *J. Mater. Eng. Perform.* **2020**, *29*, 7636–7647. [CrossRef]
36. Javidrad, H.R.; Salemi, S. Effect of the Volume Energy Density and Heat Treatment on the Defect, Microstructure, and Hardness of L-PBF Inconel 625. *Metall. Mater. Trans. A* **2020**, *51*, 5880–5891. [CrossRef]
37. Benoit, M.J.; Mazur, M.; Easton, M.A.; Brandt, M. Effect of alloy composition and laser powder bed fusion parameters on the defect formation and mechanical properties of Inconel 625. *Int. J. Adv. Manuf. Technol.* **2021**, *114*, 915–927. [CrossRef]
38. Lesyk, D.A.; Dzhemelinskyi, V.V.; Martinez, S.; Mordyuk, B.N.; Lamikiz, A. Surface Shot Peening Post-processing of Inconel 718 Alloy Parts Printed by Laser Powder Bed Fusion Additive Manufacturing. *J. Mater. Eng. Perform.* **2021**, *30*, 6982–6995. [CrossRef]
39. Wei, H.L.; Knapp, G.L.; Mukherjee, T.; DebRoy, T. Three-dimensional grain growth during multi-layer printing of a nickel-based alloy Inconel 718. *Addit. Manuf.* **2019**, *25*, 448–459. [CrossRef]
40. Taşcıoğlu, E.; Kaynak, Y.; Sharif, S.; Pıtır, F.; Suhaimi, M.A. Machining-induced surface integrity of Inconel 718 alloy fabricated by powder bed fusion additive manufacturing under various laser processing parameters. *Mach. Sci. Technol.* **2022**, *26*, 49–71. [CrossRef]
41. Schneider, J.; Lund, B.; Fullen, M. Effect of heat treatment variations on the mechanical properties of Inconel 718 selective laser melted specimens. *Addit. Manuf.* **2018**, *21*, 248–254. [CrossRef]
42. Shrivastava, A.; Kumar, S.A.; Rao, S.; Nagesha, B.K. Exploring How LPBF process parameters impact the interface characteristics of LPBF Inconel 718 deposited on Inconel 718 wrought substrates. *Opt. Laser Technol.* **2024**, *174*, 110571. [CrossRef]
43. Hwang, J.-R.; Zheng, J.-Y.; Kuo, P.-C.; Huang, C.-D.; Fung, C.-P. Process Optimization of Inconel 718 Alloy Produced by Laser Powder Bed Fusion. *Metals* **2022**, *12*, 1494. [CrossRef]
44. Vilanova, M.; Escribano-García, R.; Guraya, T.; San Sebastian, M. Optimizing Laser Powder Bed Fusion Parameters for IN-738LC by Response Surface Method. *Materials* **2020**, *13*, 4879. [CrossRef] [PubMed]
45. Muñiz-Lerma, J.A.; Tian, Y.; Wang, X.; Gauvin, R.; Brochu, M. Microstructure evolution of Inconel 738 fabricated by pulsed laser powder bed fusion. *Prog. Addit. Manuf.* **2019**, *4*, 97–107. [CrossRef]
46. Li, M.; Ma, R.; Li, L.; Ding, J.; Chang, S. Controlling texture and anisotropy in IN738LC alloy fabricated via laser powder bed fusion. *Mater. Charact.* **2024**, *218*, 114570. [CrossRef]
47. Zhang, S.; Wang, Y.; Lv, L.; Deng, H.; Bian, Q.; Hu, Q.; Tan, L.; Liu, F. Effect of powder layer thickness on the microstructure and properties of Inconel 625 superalloy manufactured by selective laser melting. *J. Alloys Compd.* **2025**, *1020*, 179465. [CrossRef]
48. Allam, A.; Alfahmi, O.; Patel, H.; Sugino, C.; Harding, M.; Ruzzene, M.; Erturk, A. Ultrasonic testing of thick and thin Inconel 625 alloys manufactured by laser powder bed fusion. *Ultrasonics* **2022**, *125*, 106780. [CrossRef] [PubMed]
49. Marchese, G.; Beretta, M.; Aversa, A.; Biamino, S. In Situ Alloying of a Modified Inconel 625 via Laser Powder Bed Fusion: Microstructure and Mechanical Properties. *Metals* **2021**, *11*, 988. [CrossRef]
50. Tian, Z.; Zhang, C.; Wang, D.; Liu, W.; Fang, X.; Wellmann, D.; Zhao, Y.; Tian, Y. A Review on Laser Powder Bed Fusion of Inconel 625 Nickel-Based Alloy. *Appl. Sci.* **2020**, *10*, 81. [CrossRef]

51. Cunningham, R.; Zhao, C.; Parab, N.; Kantzos, C.; Pauza, J.; Fezzaa, K.; Sun, T.; Rollett, A.D. Keyhole threshold and morphology in laser melting revealed by ultrahigh-speed x-ray imaging. *Science* **2019**, *363*, 849–852. [CrossRef] [PubMed]
52. Aggarwal, A.; Shin, Y.C.; Kumar, A. Unravelling keyhole instabilities and laser absorption dynamics during laser irradiation of Ti6Al4V: A high-fidelity Thermo-fluidic study. *Int. J. Heat Mass Transf.* **2024**, *219*, 124841. [CrossRef]
53. Hasanabadi, M.; Shahabad, S.I.; Keshavarzkermani, A.; Eybel, R.; Gerlich, A.; Toyserkani, E. A numerical modelling for laser Powder-bed fusion of Ti-alloy with a hybrid heat Source: An investigation on solidification and microstructure formation. *Opt. Laser Technol.* **2024**, *174*, 110647. [CrossRef]
54. Abdelmoula, M.; Musinski, W. Predicting and correlating melt pool characteristics with processing parameters in IN625 powder bed fusion Additive Manufacturing. *J. Manuf. Process.* **2024**, *121*, 427–445. [CrossRef]
55. Dai, K.; He, X.; Kong, D.; Dong, C. Multi-physical field simulation to yield defect-free IN718 alloy fabricated by laser powder bed fusion. *Mater. Lett.* **2024**, *355*, 135437. [CrossRef]
56. Shrestha, S.; Chou, K. Formation of keyhole and lack of fusion pores during the laser powder bed fusion process. *Manuf. Lett.* **2022**, *32*, 19–23. [CrossRef]
57. Lee, Y.S.; Zhang, W. Modeling of heat transfer, fluid flow and solidification microstructure of nickel-base superalloy fabricated by laser powder bed fusion. *Addit. Manuf.* **2016**, *12*, 178–188. [CrossRef]
58. Rehman, A.U.; Mahmood, M.A.; Pitir, F.; Salamci, M.U.; Popescu, A.C.; Mihailescu, I.N. Keyhole Formation by Laser Drilling in Laser Powder Bed Fusion of Ti6Al4V Biomedical Alloy: Mesoscopic Computational Fluid Dynamics Simulation versus Mathematical Modelling Using Empirical Validation. *Nanomaterials* **2021**, *11*, 3284. [CrossRef] [PubMed]
59. Semak, V.; Matsunawa, A. The Role of Recoil Pressure in Energy Balance during Laser Materials Processing. *J. Phys. D Appl. Phys.* **1997**, *30*, 2541–2552. [CrossRef]
60. Wang, X.; Wang, J.; Kang, J.; Wang, T.; Wu, P.; Feng, T.; Zheng, L.; Rong, Y. High-throughput investigation of laser powder bed fabricated Inconel 718 alloy: Fabrication, microstructure and performance. *Mater. Today Commun.* **2021**, *27*, 102303. [CrossRef]
61. Pramod, S.; Kesavan, D. Melting modes of laser powder bed fusion (L-PBF) processed IN718 alloy: Prediction and experimental analysis. *Adv. Ind. Manuf. Eng.* **2023**, *6*, 100106. [CrossRef]
62. Park, H.; Mullin, K.M.; Kumar, V.; Wander, O.; Pollock, T.M.; Zhu, Y. Resolving thermal gradients and solidification velocities during laser melting of a refractory alloy. *Addit. Manuf.* **2025**, *105*, 104750. [CrossRef]
63. Borhani, M.R.; Rajabi, M.; Razavi, R.S.; Jamaati, R. Prediction of solidification structure in the laser metal deposition of IN625 superalloy using the numerical and experimental techniques. *Mater. Today Commun.* **2024**, *40*, 109415. [CrossRef]
64. Arısoy, Y.M.; Criales, L.E.; Özel, T. Modeling and simulation of thermal field and solidification in laser powder bed fusion of nickel alloy IN625. *Opt. Laser Technol.* **2019**, *109*, 278–292. [CrossRef]
65. Huynh, T.; Mehta, A.; Graydon, K.; Woo, J.; Park, S.; Hyer, H.; Zhou, L.; Imholte, D.D.; Woolstenhulme, N.E.; Wachs, D.M.; et al. Microstructural Development in Inconel 718 Nickel-Based Superalloy Additively Manufactured by Laser Powder Bed Fusion. *Metallogr. Microstruct. Anal.* **2022**, *11*, 88–107. [CrossRef]
66. Yoshioka, J.; Eshraghi, M. Temporal evolution of temperature gradient and solidification rate in laser powder bed fusion additive manufacturing. *Heat Mass Transf.* **2023**, *59*, 1155–1166. [CrossRef]
67. Cloots, M.; Uggowitzer, P.J.; Wegener, K. Investigations on the microstructure and crack formation of IN738LC samples processed by selective laser melting using Gaussian and doughnut profiles. *Mater. Des.* **2016**, *89*, 770–784. [CrossRef]
68. Aghajani, H.; Mosayebi, M.; Pourbahari, B.; Maleksaeedi, S.; Alimehr, P.; Esmaeilizadeh, R.; Hasanabadi, M.; Bassim, N.; Toyserkani, E. Mechanistic process–microstructure–cracking correlations in laser powder bed fusion of the Ni-based superalloy IN738. *Mater. Des.* **2026**, *262*, 115504. [CrossRef]
69. Shoja Razavi, R.; Ali, K. Investigation of Geometry, Microstructure and Defect Formation in Layers Fabricated in LPBF-Processed Inconel 738LC Alloy. *Arab. J. Sci. Eng.* **2025**, *51*, 9849–9867. [CrossRef]
70. Guo, C.; Li, S.; Shi, S.; Li, X.; Hu, X.; Zhu, Q.; Ward, R.M. Effect of processing parameters on surface roughness, porosity and cracking of as-built IN738LC parts fabricated by laser powder bed fusion. *J. Mater. Process. Technol.* **2020**, *285*, 116788. [CrossRef]
71. Xu, J.; Gao, Y.; Liu, B.; Xue, S.; Hu, Y.; Ding, Y.; Zhang, D.; Lu, S.; Song, X. Improving printability of LPBF-built Inconel 738 superalloy via B-modification and high-quality powder. *Mater. Today Commun.* **2025**, *47*, 113058. [CrossRef]
72. He, Y.; Zhong, M.; Jones, N.; Beuth, J.; Webler, B. The Columnar-to-Equiaxed Transition in Melt Pools During Laser Powder Bed Fusion of M2 Steel. *Metall. Mater. Trans. A* **2021**, *52*, 4206–4221. [CrossRef]
73. Zhou, L.; Peng, Z.; Chen, J.; Ren, Y.; Niu, Y.; Qiu, W.; Tang, J.; Li, Z.; Li, C. The evolution of microstructure and mechanical properties of Inconel 625 alloy fabricated by laser powder bed fusion via novel hybrid scanning strategy. *Mater. Sci. Eng. A* **2024**, *911*, 146925. [CrossRef]
74. Liu, L.; Wang, D.; Yang, Y.; Wang, Z.; Qian, Z.; Wu, S.; Tang, J.; Han, C.; Tan, C. Effect of scanning strategies on the microstructure and mechanical properties of inconel 718 alloy fabricated by laser powder bed fusion. *Adv. Eng. Mater.* **2023**, *25*, 2200492. [CrossRef]

75. Xu, J.; Ding, Y.; Gao, Y.; Wang, H.; Hu, Y.; Zhang, D. Grain refinement and crack inhibition of hard-to-weld Inconel 738 alloy by altering the scanning strategy during selective laser melting. *Mater. Des.* **2021**, *209*, 109940. [CrossRef]
76. Marrey, M.; Eftekharian, A.; Harik, V.; Kumar, A.; Miraj, R.; Abdi, F. Additive Manufacturing of Inconel 718 by Meltpool and Grain Boundary Engineering. In *TMS 2023 152nd Annual Meeting & Exhibition Supplemental Proceedings*; TMS 2023; The Minerals, Metals & Materials Series; Springer: Cham, Switzerland, 2023. [CrossRef]
77. Chen, W.; Zhang, J.; Chen, W.; Wang, Z.; Xu, L.; Jiang, W.; Lu, H.; Fu, W. Promoting the columnar-to-equiaxed transition and grain refinement in additively manufactured Nickel-based superalloys via a short-vector localized melt-scan strategy. *J. Manuf. Process.* **2025**, *155*, 308–322. [CrossRef]
78. Schröder, J.; Evans, A.; Polatidis, E.; Čapek, J.; Mohr, G.; Serrano-Munoz, I.; Bruno, G. Understanding the impact of texture on the micromechanical anisotropy of laser powder bed fused Inconel 718. *J. Mater. Sci.* **2022**, *57*, 15036–15058. [CrossRef]
79. Gokcekaya, O.; Ishimoto, T.; Hibino, S.; Yasutomi, J.; Narushima, T.; Nakano, T. Unique crystallographic texture formation in Inconel 718 by laser powder bed fusion and its effect on mechanical anisotropy. *Acta Mater.* **2021**, *212*, 116876. [CrossRef]
80. Zhang, X.; Tu, J.; He, T.; Zhang, Q.; Liang, Y. Cascading texture evolution driven by dynamic competition of deformation mechanisms in Inconel 625 Ni-based superalloy prepared by laser powder bed fusion. *Mater. Charact.* **2025**, *229*, 115582. [CrossRef]
81. Zhu, J.; Shao, C.; Lu, F.; Feng, K.; Liu, P.; Chu, S.; Feng, Y.; Kokawa, H.; Li, Z. Origin of the anisotropic ductility and the dynamic recrystallization-like deformation behavior of laser powder bed fusion Inconel 625 at elevated temperature. *Scr. Mater.* **2022**, *221*, 114945. [CrossRef]
82. Zhou, L.; Peng, Z.; Hu, Z.; Liu, J.; Chen, J.; Ren, Y.; Niu, Y.; Qiu, W.; Chen, W.; Li, C. Grain morphology and mechanical properties tailoring of Inconel 625 alloy fabricated by laser powder bed fusion. *Adv. Eng. Mater.* **2024**, *26*, 2301785. [CrossRef]
83. Li, L.; Chen, H.; Liao, Z.; Yang, Y.; Axinte, D. Investigation of the grain deformation to orthogonal cutting process of the textured Alloy 718 fabricated by laser powder bed fusion. *Int. J. Mach. Tools Manuf.* **2023**, *190*, 104050. [CrossRef]
84. Zhong, Q.; Wei, K.; Ouyang, T.; Li, X.; Zeng, X. Effect of rotation angle on surface morphology, microstructure, and mechanical properties of Inconel 718 alloy fabricated by high power laser powder bed fusion. *J. Mater. Sci. Technol.* **2023**, *154*, 30–42. [CrossRef]
85. Serrano-Munoz, I.; Fritsch, T.; Mishurova, T.; Trofimov, A.; Apel, D.; Ulbricht, A.; Kromm, A.; Hesse, R.; Evans, A.; Bruno, G. On the interplay of microstructure and residual stress in LPBF IN718. *J. Mater. Sci.* **2020**, *56*, 5845–5867. [CrossRef]
86. Gruber, K.; Stopyra, W.; Kobiela, K.; Kohlwes, P.; Čapek, J.; Polatidis, E.; Kelbassa, I. Achieving high strength and ductility in Inconel 718: Tailoring grain structure through micron-sized carbide additives in PBF-LB/M additive manufacturing. *Virtual Phys. Prototyp.* **2024**, *19*, e2396064. [CrossRef]
87. Zhou, W.; Zhu, G.; Wang, R.; Yang, C.; Tian, Y.; Zhang, L.; Dong, A.; Wang, D.; Shu, D.; Sun, B. Inhibition of cracking by grain boundary modification in a non-weldable nickel-based superalloy processed by laser powder bed fusion. *Mater. Sci. Eng. A* **2020**, *791*, 139745. [CrossRef]
88. Jena, A.; Atabay, S.E.; Brochu, M. Microstructure and mechanical properties of crack-free Inconel 738 fabricated by laser powder bed fusion. *Mater. Sci. Eng. A* **2022**, *850*, 143524. [CrossRef]
89. Zhou, W.; Tian, Y.; Wei, D.; Tan, Q.; Kong, D.; Luo, H.; Huang, W.; Zhu, G.; Shu, D.; Mi, J.; et al. Effects of heat treatments on the microstructure and tensile properties of IN738 superalloy with high carbon content fabricated via laser powder bed fusion. *J. Alloys Compd.* **2023**, *953*, 170110. [CrossRef]
90. Hafezi, M.; Kermanpur, A.; Rezaeian, A.; Heydari, F.; Rabieifar, H.; Marchese, G.; Bassini, E.; Ugues, D.; Biamino, S. On the high-temperature tensile deformation mechanisms of the IN738LC superalloy fabricated by laser powder bed fusion. *Mater. Charact.* **2025**, *229*, 115510. [CrossRef]
91. Zhang, F.; Zhou, L.; Xie, X.; Zhang, Z.; Chao, Q.; Fan, G. Crack inhibition and crystallographic texture control in an additively manufactured IN738LC Ni-based superalloy. *J. Mater. Res. Technol.* **2024**, *33*, 652–666. [CrossRef]
92. Calandri, M.; Yin, S.; Aldwell, B.; Calignano, F.; Lupoi, R.; Ugues, D. Texture and Microstructural Features at Different Length Scales in Inconel 718 Produced by Selective Laser Melting. *Materials* **2019**, *12*, 1293. [CrossRef] [PubMed]
93. Lei, X.; Zhang, S.; Zhang, L.; Dong, N.; Wen, J.; Wu, G.; Sun, X.; Yang, F.; Rao, D.; Zhang, W.; et al. Review on Optimization of Tensile, Fatigue, and Creep Properties of Additive Manufactured Nickel-Based Superalloys by Modifying the Microstructure and Residual Stress. *Fatigue Fract. Eng. Mater. Struct.* **2026**, *49*, 3–27. [CrossRef]
94. Łach, Ł. Cellular Automata and Phase-Field Modeling of Microstructure Evolution in Metal Additive Manufacturing: Recent Advances, Hybrid Frameworks, and Pathways to Predictive Control. *Metals* **2026**, *16*, 124. [CrossRef]
95. Kumar, S.; Mukherjee, I.; Chandu, K.P.; Das, P. Multi-Phase Field Model of Laser Powder Bed Fusion Based Additive Manufacturing of IN718 Superalloy. *Adv. Theory Simul.* **2025**, *8*, 2401031. [CrossRef]
96. Prasad, A.; Yuan, L.; Lee, P.; Patel, M.; Qiu, D.; Easton, M.; StJohn, D. Towards Understanding Grain Nucleation under Additive Manufacturing Solidification Conditions. *Acta Mater.* **2020**, *195*, 392–403. [CrossRef]

97. Haines, M.; Plotkowski, A.; Frederick, C.L.; Schwalbach, E.J.; Babu, S.S. A Sensitivity Analysis of the Columnar-to-Equiaxed Transition for Ni-Based Superalloys in Electron Beam Additive Manufacturing. *Comput. Mater. Sci.* **2018**, *155*, 340–349. [CrossRef]
98. Alishavandi, M.; Orhangül, A.; Duygulu, Ö.; Güneş, H.; Ünal, R.; Salamci, M.U. Multiscale Elemental Segregation and Post-HIP Microstructural Evolution in the Laser Powder Bed Fusion of IN738LC Nickel-Based Superalloy. *Mater. Des.* **2026**, *267*, 116306. [CrossRef]
99. Lin, W.; Zhang, Z. Cracking Reduction and Texture Control in Laser Powder Bed Fusion Additive Manufactured Non-weldable Nickel Alloy. *J. Mater. Eng. Perform.* **2025**, *34*, 29290–29303. [CrossRef]
100. Paraschiv, A.; Matache, G.; Constantin, N.; Vladut, M. Investigation of Scanning Strategies and Laser Remelting Effects on Top Surface Deformation of Additively Manufactured IN 625. *Materials* **2022**, *15*, 3198. [CrossRef] [PubMed]
101. Marques, A.; Cunha, Â.; Silva, M.R.; Osendi, M.I.; Silva, F.S.; Carvalho, Ó.; Bartolomeu, F. Inconel 718 produced by laser powder bed fusion: An overview of the influence of processing parameters on microstructural and mechanical properties. *Int. J. Adv. Manuf. Technol.* **2022**, *121*, 5651–5675. [CrossRef]
102. Bryndza, G.; Tchuindjang, J.T.; Chen, F.; Habraken, A.M.; Sepúlveda, H.; Tuninetti, V.; Mertens, A.; Duchêne, L. Review of the Microstructural Impact on Creep Mechanisms and Performance for Laser Powder Bed Fusion Inconel 718. *Materials* **2025**, *18*, 276. [CrossRef] [PubMed]
103. Miao, K.; Ding, Z.; Li, R.; Ji, X.; Duan, X.; Yao, R.; Chen, P.; Wu, H. Mechanisms of Heat-Treatment-Induced Cracking in Additively Manufactured IN738 Alloy. *Materials* **2023**, *16*, 7316. [CrossRef] [PubMed]
104. Kim, K.; Kang, T.; Lee, K. Influence of Post-Heat Treatments on the Microstructure, Mechanical Responses of IN738LC Superalloy Manufactured via Laser Powder Bed Fusion. *Adv. Eng. Mater.* **2023**, *25*, 2201098. [CrossRef]
105. Hu, Y.; Jia, H.; Zhang, X.; Yang, X.; Zhang, D. Delayed recrystallization behavior and deformation mechanism of IN738LC alloy prepared by laser powder bed fusion. *Mater. Sci. Eng. A* **2024**, *903*, 146697. [CrossRef]
106. Zhu, J.; Xu, J.; Kokawa, H.; Zhao, Y.; Feng, K.; Li, Z.; Ramamurty, U. Suppression of epitaxial grain growth in laser powder bed fusion fabricated Inconel 625 through intermittent variation of the build layer thickness. *Mater. Sci. Eng. A* **2023**, *886*, 145679. [CrossRef]
107. Tajyar, A.; Brooks, N.; Holtham, N.; Rowe, R.; Newell, D.J.; Palazotto, A.N.; Davami, K. Effects of a modified heat-treatment on microstructure and mechanical properties of additively manufactured Inconel 718. *Mater. Sci. Eng. A* **2022**, *838*, 142770. [CrossRef]
108. Perez-Ruiz, J.D.; Velilla-Díaz, W.; Abasolo, M.; Gómez Escudero, G.; López de Lacalle, L.N. Effect of Microstructure and Crystallographic Texture on the Fracture Toughness Anisotropy of LPBF IN718. *Materials* **2025**, *18*, 3737. [CrossRef] [PubMed]
109. Liu, J.; Zhou, L.; Peng, Z.; Chen, B.; Tan, Y.; Chen, J.; Huang, W.; Li, C. Anisotropy Evolution of Tensile Properties in Laser Powder Bed Fusion-Fabricated Inconel 625 Alloy at High Temperature. *Acta Metall. Sin. Engl. Lett.* **2025**, *38*, 555–569. [CrossRef]
110. Chen, Y.; Wang, W.; Ou, Y.; Chang, H.; Wu, Y.; Yang, R.; Zhai, Z.; Li, K.; Shen, L. Microstructure and mechanical property comparison of Inconel alloys fabricated using micro and conventional laser powder bed fusion. *Mater. Des.* **2024**, *237*, 112534. [CrossRef]
111. Demir, A.G.; Mazzoleni, L.; Caprio, L.; Pacher, M.; Previtali, B. Complementary use of pulsed and continuous wave emission modes to stabilize melt pool geometry in laser powder bed fusion. *Opt. Laser Technol.* **2019**, *113*, 15–26. [CrossRef]
112. Trejos-Taborda, J.; Reyes-Osorio, L.; Garza, C.; Zambrano-Robledo, P.d.C.; Lopez-Botello, O. Finite element modeling of melt pool dynamics in laser powder bed fusion of 316L stainless steel. *Int. J. Adv. Manuf. Technol.* **2022**, *120*, 3947–3961. [CrossRef]
113. Yang, L.; Lo, L.; Ding, S.; Özel, T. Monitoring and detection of meltpool and spatter regions in laser powder bed fusion of super alloy Inconel 625. *Prog. Addit. Manuf.* **2020**, *5*, 367–378. [CrossRef]
114. Ramakrishna, M.; Koppoju, S.; Telasang, G.; Korla, R.; Padmanabham, G. Effect of Solutionizing Temperature on the Microstructural Evolution during Double Aging of Powder Bed Fusion-Additive Manufactured IN718 Alloy. *Mater. Charact.* **2021**, *172*, 110868. [CrossRef]
115. Guo, C.; Li, G.; Zhou, F.; Li, X.; Xu, Z.; Liu, C.; Hu, X.; Lu, H.; Li, Z.; Zhu, Q. Understanding the Significant Effect of Boron Content on the Printability of IN738LC Superalloy Fabricated Using Laser Powder Bed Fusion. *Opt. Laser Technol.* **2023**, *159*, 108954. [CrossRef]
116. Gullipalli, C.; Thawari, N.; Burad, P.; Gupta, T.V.K. Residual stresses and distortions in additive manufactured Inconel 718. *Mater. Manuf. Process.* **2023**, *38*, 1549–1560. [CrossRef]
117. Serrano-Munoz, I.; Ulbricht, A.; Fritsch, T.; Mishurova, T.; Kromm, A.; Hofmann, M.; Wimpory, R.C.; Evans, A.; Bruno, G. Scanning Manufacturing Parameters Determining the Residual Stress State in LPBF IN718 Small Parts. *Adv. Eng. Mater.* **2021**, *23*, 2100158. [CrossRef]
118. Hyer, H.; Newell, R.; Matejczyk, D.; Hsie, S.; Anthony, M.; Zhou, L.; Kammerer, C.; Sohn, Y. Microstructural Development in As Built and Heat Treated IN625 Component Additively Manufactured by Laser Powder Bed Fusion. *J. Phase Equilibria Diffus.* **2021**, *42*, 14–27. [CrossRef]

119. Song, Z.; Gao, S.; Wang, Z.; Lan, L.; Hou, J.; He, B. Effects of non-equilibrium microstructures on microstructure evolution and mechanical properties of laser powder bed fusion IN625 Ni-based superalloy during long-term thermal exposure at 700 C and 750 C. *Mater. Sci. Eng. A* **2022**, *856*, 143883. [CrossRef]
120. Kikukawa, T.; Ishimoto, T.; Kim, H.S.; Nakano, T. Remarkable strengthening effects of cells in laser powder bed fusion-processed Inconel 718. *Mater. Res. Lett.* **2025**, *13*, 837–843. [CrossRef]
121. Menon, N.; Mahdi, T.H.; Basak, A. Microstructure of IN738LC Fabricated Using Laser Powder Bed Fusion Additive Manufacturing. *ASME. J. Turbomach.* **2022**, *144*, 031011. [CrossRef]
122. Ledwig, P.; Pasiowiec, H.; Cichocki, K.; Lisiecka-Graca, P.; Gola, K.; Wróbel, R.; Dubiel, B. Tailoring Microstructure and Mechanical Properties of Additively Manufactured Inconel 625 by Remelting Strategy in Laser Powder Bed Fusion. *Metall. Mater. Trans. A* **2024**, *55*, 2485–2508. [CrossRef]
123. Sanchez, S.; Hyde, C.J.; Ashcroft, I.A.; G.A., R.; Clare, A.T. Multi-laser scan strategies for enhancing creep performance in LPBF. *Addit. Manuf.* **2021**, *41*, 101948. [CrossRef]
124. Meng, T.L.; Gong, N.; Chan, W.L.; Karyappa, R.; Wei, Y.; Cheng, H.K.F.; Liu, H. On Porosity and Its Mitigation and Closure in Additively Manufactured Alloys. In *Proceedings of the 3rd International Conference on Advanced Surface Enhancement (INCASE) 2023*; Maharjan, N., He, W., Eds.; INCASE 2023; Lecture Notes in Mechanical Engineering; Springer: Singapore, 2023. [CrossRef]
125. Mohan, R.V.; Ingle, N. Prediction of Porosity and its Mechanisms in Metal Additive Manufacturing ASME International Mechanical Engineering Congress and Exposition. *Am. Soc. Mech. Eng.* **2022**, *86656*, V003T03A051. [CrossRef]
126. Salarian, M.; Asgari, H.; Vlasea, M. Pore space characteristics and corresponding effect on tensile properties of Inconel 625 fabricated via laser powder bed fusion. *Mater. Sci. Eng. A* **2020**, *769*, 138525. [CrossRef]
127. Dwivedi, A.; Khurana, M.K.; Bala, Y.G. A comparative study of porosity rate measurement methods and influence of energy density in Inconel 718 produced by laser powder bed fusion additive manufacturing process. *Int. J. Interact. Des. Manuf.* **2024**, *19*, 2645–2658. [CrossRef]
128. Sanchez, S.; Gaspard, G.; Hyde, C.J.; Ashcroft, I.A.; G.A., R.; Clare, A.T. The creep behaviour of nickel alloy 718 manufactured by laser powder bed fusion. *Mater. Des.* **2021**, *204*, 109647. [CrossRef]
129. Jiang, C.-P.; Masrurotin Wibisono, A.T.; Macek, W.; Ramezani, M. Enhancing Internal Cooling Channel Design in Inconel 718 Turbine Blades via Laser Powder Bed Fusion: A Comprehensive Review of Surface Topography Enhancements. *Int. J. Precis. Eng. Manuf.* **2024**, *26*, 487–511. [CrossRef]
130. Abarca, M.J.; Darabi, R.; de Sa, J.C.; Parente, M.; Reis, A. Multi-scale modeling for prediction of residual stress and distortion in Ti–6Al–4V semi-circular thin-walled parts additively manufactured by laser powder bed fusion (LPBF). *Thin-Walled Struct.* **2023**, *182*, 110151. [CrossRef]
131. Olleak, A.; Xi, Z. A study of modeling assumptions and adaptive remeshing for Thermomechanical finite element modeling of the LPBF process. *Int. J. Adv. Manuf. Technol.* **2021**, *115*, 3599–3615. [CrossRef]
132. Santi, A.; Bayat, M.; Hattel, J. Multiphysics modeling of metal based additive manufacturing Processes with focus on Thermomechanical conditions. *J. Therm. Stress.* **2023**, *46*, 445–463. [CrossRef]
133. Carraturo, M.; Viguerie, A.; Reali, A.; Auricchio, F. Two-level method part-scale thermal analysis of laser powder bed fusion Additive Manufacturing. *Eng. Comput.* **2022**, *38*, 4815–4828. [CrossRef]
134. Łach, Ł.; Svyetlichnyy, D. Advanced Numerical Modeling of Powder Bed Fusion: From Physics-Based Simulations to AI-Augmented Digital Twins. *Materials* **2026**, *19*, 426. [CrossRef] [PubMed]
135. Zinovieva, O.; Romanova, V.; Dymnich, E.; Zinoviev, A.; Balokhonov, R. A Review of Computational Approaches to the Microstructure-Informed Mechanical Modelling of Metals Produced by Powder Bed Fusion Additive Manufacturing. *Material* **2023**, *16*, 6459. [CrossRef] [PubMed]
136. Shen, T.; Li, B. Digital twins in additive manufacturing: A state-of-the-art review. *Int. J. Adv. Manuf. Technol.* **2024**, *131*, 63–92. [CrossRef]
137. Sharma, S.; Joshi, S.S.; Pantawane, M.V.; Radhakrishnan, M.; Mazumder, S.; Dahotre, N.B. Multiphysics multi-scale computational framework for linking process–structure–property relationships in metal additive manufacturing: A critical review. *Int. Mater. Rev.* **2023**, *68*, 943–1009. [CrossRef]
138. Kolate, V.D.; Chaudhary, M.K.; Mane, S.; Devadhe, M. Digital twin–enabled model predictive control in additive manufacturing: Critical review, research challenges, and future directions. *Mater. Manuf. Process.* **2025**, *41*, 1–17. [CrossRef]
139. Ben Amor, S.; Elloumi, N.; Eltaief, A.; Louhichi, B.; Alrasheedi, N.H.; Seibi, A. Digital Twin Implementation in additive manufacturing: A Comprehensive Review. *Processes* **2024**, *12*, 1062. [CrossRef]
140. Hashemi, S.M.; Parvizi, S.; Baghbanijavid, H.; Tan, A.T.L.; Nematollahi, M.; Ramazani, A.; Fang, N.X.; Elahinia, M. Computational modelling of process–structure–property–performance relationships in metal additive manufacturing: A review. *Int. Mater. Rev.* **2021**, *67*, 1–46. [CrossRef]
141. Sow, M.; De Terris, T.; Castelnau, O.; Hamouche, Z.; Coste, F.; Fabbro, R.; Peyre, P. Influence of beam diameter on Laser Powder Bed Fusion (L-PBF) process. *Addit. Manuf.* **2020**, *36*, 101532. [CrossRef]

142. Mirzabeigi, N.; Holfelder-Schwalme, P.; He, Y.; Wudy, K. Tailored microstructure in laser-based powder bed fusion of IN718 through novel beam shaping technology. *J. Laser Appl.* **2024**, *36*, 4. [CrossRef]
143. Raut, R.; Basak, A. Thermal Deformation Analysis of Large-Scale High-Aspect-Ratio Parts Fabricated Using Multi-Laser Powder Bed Fusion. *J. Exp. Theor. Anal.* **2026**, *4*, 6. [CrossRef]
144. Peng, J.; Jiang, W.-G.; Ling, P.-H.; Wang, H.-T. A conceptual multi-laser integration technology for significantly reducing porosity and residual stress in Inconel 718 parts fabricated by laser powder bed fusion. *Opt. Laser Technol.* **2025**, *184*, 112557. [CrossRef]
145. Ball, A.K.; Basak, A. Numerical investigation of the thermal distortion in multi-laser powder bed fusion (ML-PBF) additive manufacturing of inconel 625. *Chin. J. Mech. Eng. Addit. Manuf. Front.* **2023**, *2*, 100103. [CrossRef]
146. Rindler, J.; Slone, C.; Herderick, E.; Mills, M.; Ramirez, A. Investigation on the potential effects of laser stitching and subsequent heat treatment on the microstructure and mechanical properties of Nickel Alloy 718 produced via Laser Powder Bed Fusion (L-PBF). *Addit. Manuf.* **2022**, *57*, 102906. [CrossRef]
147. Aydogan, B.; Chou, K. Review of In Situ Detection and Ex Situ Characterization of Porosity in Laser Powder Bed Fusion Metal Additive Manufacturing. *Metals* **2024**, *14*, 669. [CrossRef]
148. Grasso, M.L.G.; Remani, A.; Dickins, A.; Colosimo, B.M.; Leach, R.K. In-situ measurement and monitoring methods for metal powder bed fusion: An updated review. *Meas. Sci. Technol.* **2021**, *32*, 112001. [CrossRef]
149. Gould, B.; Wolff, S.; Parab, N.; Zhao, C.; Lorenzo-Martin, M.C.; Fezzaa, K.; Greco, A.; Sun, T. In Situ Analysis of Laser Powder Bed Fusion Using Simultaneous High-Speed Infrared and X-ray Imaging. *JOM* **2020**, *73*, 201–211. [CrossRef]
150. Grasso, M.; Colosimo, B.M. Process defects and in situ monitoring methods in metal powder bed fusion: A review. *Meas. Sci. Technol.* **2017**, *28*, 044005. [CrossRef]
151. Parab, N.D.; Zhao, C.; Cunningham, R.; Escano, L.I.; Gould, B.; Wolff, S.; Guo, Q.; Xiong, L.; Kantzos, C.; Pauza, J.; et al. High-speed Synchrotron X-ray Imaging of Laser Powder Bed Fusion Process. *Synchrotron Radiat. News* **2019**, *32*, 4–8. [CrossRef]
152. Mahmoud, D.; Magolon, M.; Boer, J.; Elbestawi, M.A.; Mohammadi, M.G. Applications of Machine Learning in Process Monitoring and Controls of L-PBF additive manufacturing: A Review. *Appl. Sci.* **2021**, *11*, 11910. [CrossRef]
153. Mahmood, M.; Tariq, U. A novel framework using FEM and machine learning models with experimental verification for Inconel-718 rapid part qualification by laser powder bed fusion. *Int. J. Adv. Manuf. Technol.* **2023**, *129*, 1567–1584. [CrossRef]
154. Murzin, S.P. Artificial Intelligence-Driven Innovations in Laser Processing of Metallic Materials. *Metals* **2024**, *14*, 1458. [CrossRef]
155. Herzog, T.; Brandt, M.; Trinchi, A.; Sola, A.; Molotnikov, A. Process monitoring and machine learning for defect detection in laser-based metal additive manufacturing. *J. Intell. Manuf.* **2023**, *35*, 1407–1437. [CrossRef]
156. Pandiyan, V.; Wróbel, R.; Leinenbach, C.; Shevchik, S. Optimizing in-situ monitoring for laser powder bed fusion process: Deciphering acoustic emission and sensor sensitivity with explainable machine learning. *J. Mater. Process. Technol.* **2023**, *321*, 118144. [CrossRef]
157. Sun, X.; Chen, M.; Liu, T.; Zhang, K.; Wei, H.; Zhu, Z.; Liao, W. Characterization, preparation, and reuse of metallic powders for laser powder bed fusion: A review. *Int. J. Extrem. Manuf.* **2024**, *6*, 012003. [CrossRef]
158. Rock, C.; Ledford, C.; Garcia-Avila, M.; West, H.; Miller, V.M.; Pankow, M.; Dehoff, R.; Horn, T. The Influence of Powder Reuse on the Properties of Nickel Super Alloy ATI 718™ in Laser Powder Bed Fusion Additive Manufacturing. *Metall. Mater. Trans. B* **2021**, *52*, 676–688. [CrossRef]
159. Kong, D.-C.; Dong, C.-F.; Ni, X.-Q.; Zhang, L.; Li, R.-X.; He, X.; Man, C.; Li, X.-G. Microstructure and mechanical properties of nickel-based superalloy fabricated by laser powder-bed fusion using recycled powders. *Int. J. Miner. Metall. Mater.* **2021**, *28*, 266–278. [CrossRef]
160. Huang, T.X.; Liu, Z.; Jiang, D.; Ye, S.; Liu, T.; Zhou, R.; Zhang, Y. Laser beam powder bed fusion nickel-based superalloys: Microstructure, alloy tailoring and mechanical properties. *Virtual Phys. Prototyp.* **2026**, *21*, e2619387. [CrossRef]
161. Chowdhury, H.T.; Palleda, T.N.; Kakuta, N.; Kakehi, K. Effects of Preheating on Thermal Behavior in Inconel 718 Processed by Additive Manufacturing. *Thermo* **2024**, *4*, 48–64. [CrossRef]
162. Mostafaei, A.; Ghiaasiaan, R.; Ho, I.-T.; Strayer, S.; Chang, K.-C.; Shamsaei, N.; Shao, S.; Paul, S.; Yeh, A.-C.; Tin, S.; et al. Additive Manufacturing of Nickel-Based Superalloys: A State-of-the-Art Review on Process-Structure-Defect-Property Relationship. *Prog. Mater. Sci.* **2023**, *136*, 101108. [CrossRef]
163. Abdelwahed, M.; Puchades, J.R.B.; Griñán, L.P.; Ceniceros, M.M.; Rovatti, L.; Ishola, R.M.; Vedani, M. Cracking Mechanisms and Effect of Extensive Preheating in CM247LC and IN713LC Ni-Base Superalloy Processed by Laser Powder Bed Fusion. *Mater. Today Commun.* **2023**, *37*, 107644. [CrossRef]
164. Adegoke, O.; Andersson, J.; Brodin, H.; Pederson, R. Review of Laser Powder Bed Fusion of Gamma-Prime-Strengthened Nickel-Based Superalloys. *Metals* **2020**, *10*, 996. [CrossRef]

Disclaimer/Publisher's Note: The statements, opinions and data contained in all publications are solely those of the individual author(s) and contributor(s) and not of MDPI and/or the editor(s). MDPI and/or the editor(s) disclaim responsibility for any injury to people or property resulting from any ideas, methods, instructions or products referred to in the content.